Optical control of muscular nicotinic channels with azocuroniums, photoswitchable azobenzenes bearing two *N*-methyl-*N*-carbocyclic quaternary ammonium groups

Clara Herrera-Arozamena, Martín Estrada-Valencia, Olaia Martí-Marí, Concepción Pérez, Mario de la Fuente Revenga, Carlos A. Villalba-Galea, María Isabel Rodríguez-Franco

PII: S0223-5234(20)30373-1

DOI: https://doi.org/10.1016/j.ejmech.2020.112403

Reference: EJMECH 112403

To appear in: *European Journal of Medicinal Chemistry*

Received Date: 11 February 2020

Revised Date: 17 April 2020

Accepted Date: 27 April 2020

Please cite this article as: C. Herrera-Arozamena, Martí. Estrada-Valencia, O. Martí-Marí, Concepció. Pérez, M. de la Fuente Revenga, C.A. Villalba-Galea, Marí.Isabel. Rodríguez-Franco, Optical control of muscular nicotinic channels with azocuroniums, photoswitchable azobenzenes bearing two *N*-methyl-*N*-carbocyclic quaternary ammonium groups, *European Journal of Medicinal Chemistry* (2020), doi: https://doi.org/10.1016/j.ejmech.2020.112403.

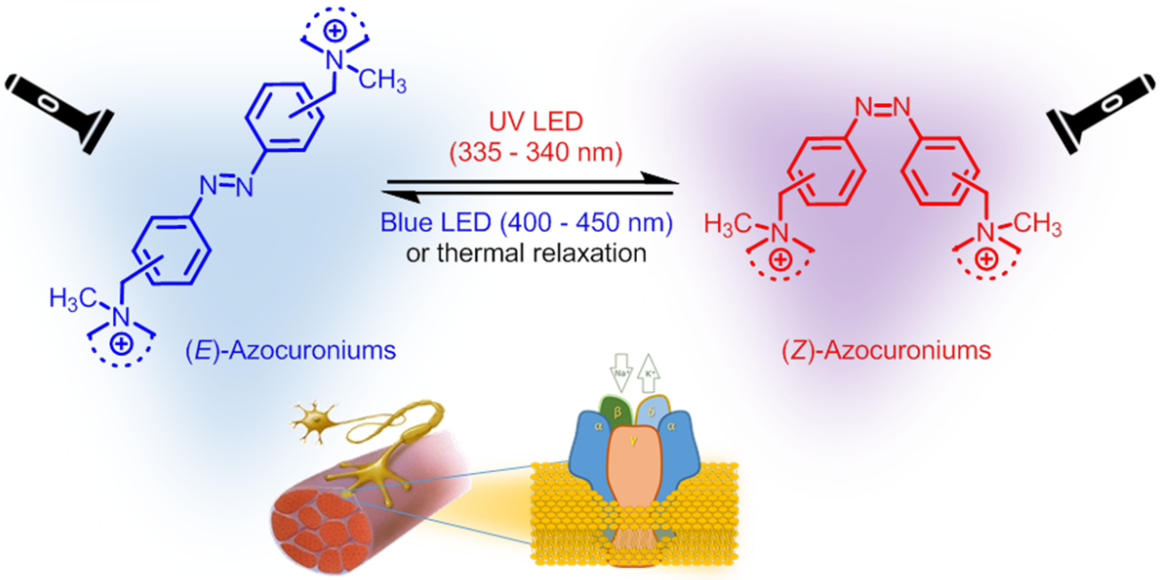
UV LED
(335 - 340 nm)
Blue LED (400 - 450 nm)
or thermal relaxation
(E)-Azocuroniums
(Z)-Azocuroniums

Optical control of muscular nicotinic channels with azocuroniums, photoswitchable azobenzenes bearing two *N*-methyl-*N*-carbocyclic quaternary ammonium groups

Clara Herrera-Arozamena[a], Martín Estrada-Valencia[a], Olaia Martí-Marí[a], Concepción Pérez[a], Mario de la Fuente Revenga[b], Carlos A. Villalba-Galea[c,*], and María Isabel Rodríguez-Franco[a,*]

[a]Instituto de Química Médica, Consejo Superior de Investigaciones Científicas (IQM-CSIC), c/ Juan de la Cierva 3, E-28006 Madrid, Spain.

[b]Department of Physiology and Biophysics, School of Medicine, Virginia Commonwealth University, Richmond, VA 23298, USA

[c]Physiology and Pharmacology Department, University of the Pacific, Stockton, CA, USA.

*Correspondence should be addressed to:
María Isabel Rodríguez-Franco
Instituto de Química Médica (IQM-CSIC)
C/ Juan de la Cierva, 3. 28006
Madrid, Spain.
Email: isabelrguez@iqm.csic.es
ORCID: 0000-0002-6500-792X

Carlos A. Villalba-Galea
Department of Physiology and Pharmacology
Thomas J. Long School of Pharmacy & Health Sciences
University of the Pacific
3601 Pacific Avenue
Stockton, CA 95211, USA
Email: cvillalbagalea@pacific.edu

Keywords

Photoswitchable neuromuscular ligands

Muscle-type nicotinic receptors

Electrophysiological studies

Structure-activity relationships

Highlights

- Azocuroniums: azobenzene plus two *N*-methyl-*N*-carbocyclic quaternary ammonium groups
- Azocuroniums are easily (*E*)/(*Z*)-photoisomerized by irradiation at blue or UV-LED
- *m*-Azocuroniums: more potent and selective in muscular nAChR than *p*-azocuroniums
- *m*-Azocuroniums are selective ligands of muscle-type nAChRs *vs.* neuronal nAChRs
- *m*-Azocuroniums are muscular nAChR antagonists, except the pyrrolidine derivative

Abbreviations

ACh, acetylcholine; nAChRs: nicotinic acetylcholine receptors; bisQ, 3,3'-bis[α-(trimethylammonium)methyl]azobenzene; GPCRs, G protein-coupled receptors; LED: light-emitting diode; NMBAs, neuromuscular blocking agents; TEVC, two-electrode voltage-clamp technique.

ABSTRACT

By linking two *N*-methyl-*N*-carbocyclic quaternary ammonium groups to an azobenzene scaffold in *meta*- or *para*-positions we generated a series of photoswitchable neuromuscular ligands for which we coined the term "azocuroniums". These compounds switched between the (*E*)- and (*Z*)-isomers by light irradiation at 400-450 nm and 335-340 nm, respectively. *Meta*-azocuroniums were potent nicotinic ligands with a clear selectivity for the muscular nAChRs compared to neuronal α7 and α4β2 subtypes, showed good solubility in physiologic media, negligible cell toxicity, and would not reach the CNS. Electrophysiological studies in muscle-type nAChRs expressed in *Xenopus laevis* oocytes showed that (*E*)-isomers were more potent than (*Z*)-forms. All *meta*-azocuroniums were neuromuscular blockers, with the exception of the pyrrolidine derivative that was an agonist. These new *meta*-azocuroniums, which can be modulated *ad libitum* by light, could be employed as photoswitchable muscle relaxants with fewer side effects for surgical interventions and as tools to better understand the pharmacology of muscle-type nAChRs.

1. Introduction

Nicotinic acetylcholine receptors (nAChRs) are ligand-gated ion-channels physiologically activated by acetylcholine (ACh), which consist of five protein subunits organized around a central pore. They constitute a superfamily of receptors that are critically involved in cellular electrical signaling in the nervous and skeletomuscular systems. In general, nAChRs are found in either neurons or skeletal muscles, confined in synapses where they relay unidirectional electrical information from one cell to another. Neuronal nAChRs are made by combinations of alpha (α2-α10) and beta subunits (β2-β4) with variable stoichiometry or by alpha homo-pentamers (α7-α9). In the mammalian brain the most common neuronal subtypes are α7 and α4β2 nAChRs, which are involved in numerous physiological functions such as cognition, learning and memory, physical stimulation, cerebral blood flow and metabolism [1,2].

In contrast to the neuronal counterparts, muscular nAChRs are composed of four types of proteins: two α1, one β1 and one gamma (γ) subunits, accompanied by either an epsilon (ε) or a delta (δ) subunit, depending on the developmental stage of the muscle [3,4]. Embryonic muscle receptors have a δ subunit, whereas in adults the ε type is present [5,6]. In skeletal muscles, nAChRs are confined within the end-plate terminal, which is made of specialized synapses linking a motor neuron to individual muscle fibers. Activation of nAChRs initiates the electrical signal that triggers action potentials, leading to muscle contraction.

Natural extracts containing neuromuscular blocking agents (NMBAs), such as curare alkaloids, have been used for centuries by South American indigenous tribes for hunting.

Many plant extract derived-NMBAs have been identified, purified and used as leads in the development of muscle relaxants for surgical procedures and other applications, including cosmetics (Figure 1). Despite the benefits that these compounds may offer in clinic, some of them are known to produce adverse side-effects in patients. For instance, the aminosteroid pancuronium is a synthetic curare-mimetic used as a muscle relaxant to facilitate endotracheal intubation, which causes several undesirable effects such as tachycardia, increase in blood pressure, respiratory depression, and apnea [7]. In this context, we recognized that the development of novel NMBAs analogues with manageable or null side-effects would produce safer new drugs for surgical interventions and also provide a breakthrough in understanding the pharmacology of muscle nAChRs. Towards this ideal outcome, we set out to design novel ligands for nAChRs that, in addition to their selectivity towards muscular subtypes, they have photoswitchable properties so that they can be activated and deactivated by light irradiation at different wavelengths. The quick modulation of the biological activity of the photoisomerizable compounds by light allows a fine adjustment of their spatial and temporal activity, which can hardly be achieved with non-photoswitchable ligands [8].

Each muscular nAChR has two binding sites for ACh in the extracellular domain, at αδ and either αε or αγ subunit interfaces. In these interfaces, aromatic residues (tryptophan and tyrosine) provide negative π-electron clouds that can electrostatically interact with the positively charged ammonium group [$-N^{+}(CH_3)_3$] of the neurotransmitter ACh [9,10]. In these receptors, the cation-π interaction is essential for binding and action. Regarding the quaternary ammonium group, it is known that compounds with less sterically hindered amino groups tend to be agonists, such as carbachol, suxamethonium, and bisQ. In contrast,

compounds with larger and hydrophobic substitutions, including *N*-carbocycle groups tend to be antagonists, such as the case of benzylisoquinoliniums (e.g., atracurium, mivacurium and cisatracurium) or aminosteroids (e.g., pancuronium, rocuronium and vecuronium) (Figure 1) [11,12].

In the early 1970s, the Erlanger's group reported that bisQ activates nicotinic receptors in the electroplax of electric fish *Electrophorus electricus*. As other azobenzene-based compounds, bisQ is photo-isomerizable, being a potent nAChR activator when it is a (*E*)-isomer, but not while being a (*Z*)-isomer [13,14]. From these pioneer studies many photoswitchable ligands have been developed and applied to a wide range of biological targets, such as G protein-coupled receptors (GPCRs), ion channels, kinases, proteases, etc [15-22]. Therapeutic efficacies of photo-isomerizable compounds have been demonstrated on the cellular level and some studies have progressed to live animals, such as the vision restoration with diazene-based photoswitchable drugs in blind mice [23-26].

In recent years, new photoswitchable nicotinic ligands have been developed by adding a single trimethylammonium head to one extreme of azobenzene scaffolds [27-29]. This strategy produced preferentially agonists, with selectivity for activating neuronal nAChRs compared to muscle-type receptors. For example, the trimethylammonium derivative azocholine is a selective photoswitchable agonist for neuronal α7 nAChRs compared to muscular receptors [30].

Our group is now interested in developing new neuromuscular blockers that, in addition to their photoswitchable properties, displayed selectivity towards muscle-type nAChRs compared to neuronal receptors. From bibliographic precedents, we rationalized that we

could generate photoswitchable antagonists for muscular nAChRs by the replacement of two methyl groups of both quaternary ammonium groups of the muscle agonist bisQ by *N*-carbocycles, commonly present in curare NMBAs. As a proof of principle, here we have designed, synthesized, and tested a series of novel muscular nAChR ligands, named azocuroniums (**1**) due to their structural similarity to curare-like drugs, the activity of which can be easily modulated by light (Figure 1) and which functional character depends on some structural features evaluated here.

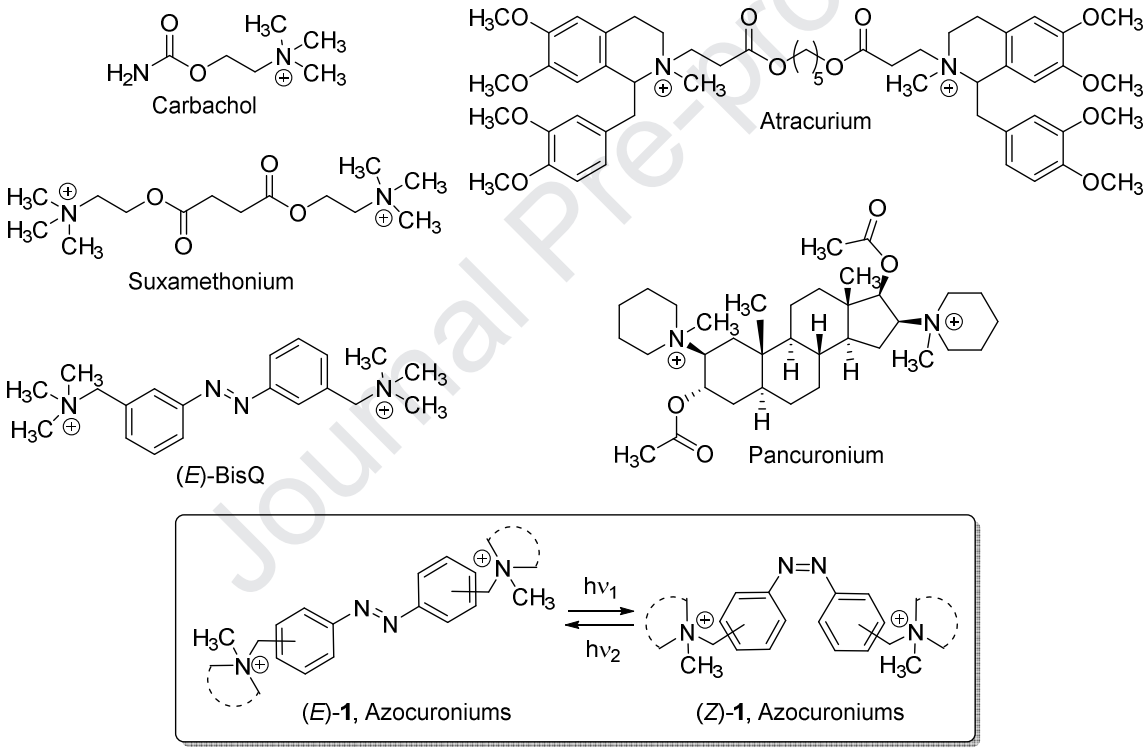

Figure 1. Structures of muscle-type nAChRs agonists (carbachol, suxamethonium and (*E*)-bisQ) and antagonists (atracurium and pancuronium). General structure of the new azocuroniums (**1**) on their (*E*)- and (*Z*)-isomers.

2. Results and discussion

2.1. Synthesis of azocuroniums

Reaction of commercially available *meta*- or *para*-nitrobenzyl bromide (1 equiv.) with the corresponding amine (pyrrolidine, piperidine, azepane, or 1,2,3,6-tetrahydropyridine) (1.2 equiv.) in basic conditions under mw irradiation at 120 °C for 10 min, gave the corresponding nitro derivative *m*-**2**(**a**-**d**) and *p*-**2**(**a**,**b**) in excellent yield (91-99%) (Scheme 1). The subsequent treatment of these nitro compounds with a solution of $LiAlH_4$ in diethyl ether (5 equiv.) afforded the required azobenzenes *m*-**3**(**a**-**d**) and *p*-**3**(**a**,**b**), in one-step and in moderate to excellent yields (61-97%). Asymmetric azocompound *m*-**4b** was synthesized from 3-(piperidin-1-ylmethyl)aniline [31] and commercial nitrosobenzene in high yield (93%) by a Mills reaction. All azo intermediates *m*-**3**(**a**-**d**), *p*-**3**(**a**,**b**) and *m*-**4b** were purified by preparative thin-layer chromatography (TLC), obtaining the (*E*)-isomer as the major isomer, as deduced from HPLC-MS and NMR data [see (*E*) / (*Z*)-ratio in Scheme 1].

Then, the intermediate tertiary amines were methylated with CH_3I (1.3 equiv.) at 120 °C for 12 min. under mw irradiation, obtaining the desired quarternary ammonium azobenzenes *m*-**1**(**a**-**d**), *p*-**1**(**a**,**b**) and *m*-**5b**, which were purified by crystallization from methanol. Remarkably, these azocuronium salts were isolated in their (*E*)-forms in high isomeric purity, equal or greater than 95% [see (*E*) / (*Z*)-ratio in Scheme 1]. This fact could be the result of the sum of a high temperature (120 ºC) in the mw-oven, which could favor the formation of the thermodynamically more stable (*E*)-isomer, and the crystallization process, which could enrich the major species.

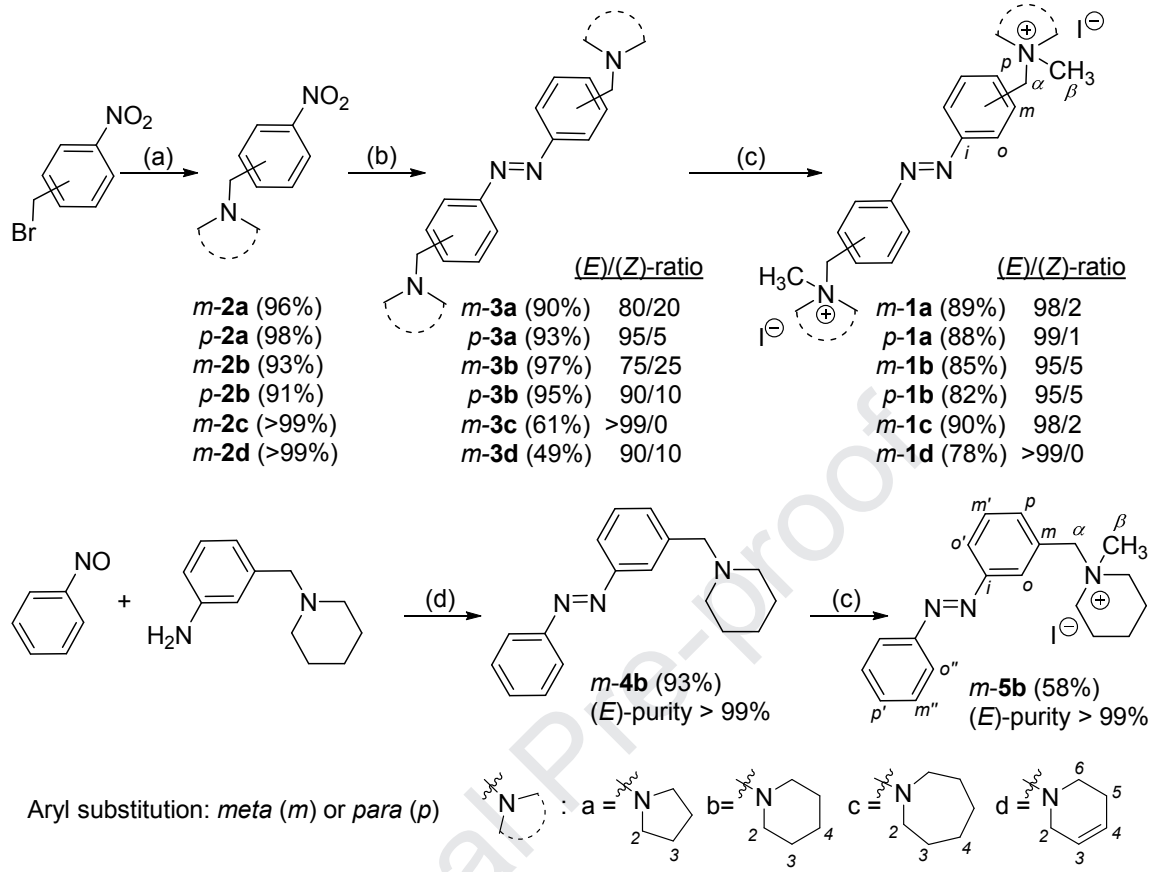

Scheme 1. Reagents and conditions: (a) Amine (pyrrolidine, piperidine, azepane, or 1,2,3,6-tetrahydropyridine) (1.2 equiv.), K_2CO_3, acetone, mw, 120 ºC, 10 min; (b) $LiAlH_4$ in Et_2O (5 equiv.), N_2, -78 °C to rt; (c) CH_3I (1.3 equiv.), DMF, mw, 120 ºC, 12 min; (d) Acetic acid, toluene, 60 ºC, overnight.

All compounds were characterized by their analytical (HPLC, HRMS) and spectroscopic data (^{1}H NMR, ^{13}C NMR). Complete NMR assignment of their hydrogen and carbon atoms were made by ^{1}H – ^{13}C two-dimensional diagrams, mainly HSQC (heteronuclear single quantum correlation) and HMBC (heteronuclear multiple bond correlation) (See Supplementary Information for further details).

2.2. Evaluation of thermodynamic solubility, in vitro CNS-penetration (PAMPA-BBB assay), and cell toxicity

The thermodynamic solubility of azocuronium salts *m*-**1**(**a**-**d**), *p*-**1**(**a**,**b**) and *m*-**5b** was determined in pH 7.4 phosphate 45 mM buffer following described protocols [32,33] (Table 1). As expected and due to their ionic character, in physiological medium all azocuronium salts showed high solubility values (5.5 – 38.4 mM). Remarkably, all *meta*-derivatives were found to be more soluble than their *para*- counterparts, probably due to the higher polarity of the former.

Table 1. Thermodynamic solubility (mM) in water at pH 7.4 and *in vitro* CNS permeability data of azocuroniums *m*-**1**(**a**-**d**), *p*-**1**(**a**,**b**) and *m*-**5b**.[a]

	Solubility at pH 7.4 (mM)	PAMPA-BBB (P_e, 10^{-6} cm s^{-1})
m-**1a**	36.3 ± 3.1	< 1.0 (cns -)
p-**1a**	14.8 ± 1.2	< 1.0 (cns -)
m-**1b**	38.4 ± 3.5	< 1.0 (cns -)
p-**1b**	34.9 ± 3.2	< 1.0 (cns -)
m-**1c**	5.9 ± 0.5	< 1.0 (cns -)
m-**1d**	16.3 ± 0.1	< 1.0 (cns -)
m-**5b**	5.5 ± 0.1	2.0 ± 0.2 (cns +/-)

[a]Results are the mean ± SD of three independent experiments. [b]Predictive CNS penetration: cns- denotes compounds that are no able to penetrate into the CNS; cns +/- denotes uncertain CNS penetration.

To check if new azocuroniums *m*-**1**(**a-d**), *p*-**1**(**a**,**b**) and *m*-**5b** could be able to reach the CNS, we used the *in vitro* parallel artificial membrane permeability assay to model the blood-brain barrier (PAMPA-BBB) described by Di et al. [34], and partially modified and validated by us [35-40]. The passive CNS-permeation of azocuroniums through a lipid extract of porcine brain was measured at rt. In each experiment, 11 commercial drugs of known brain permeability were also tested and their permeability values normalized to the reported PAMPA-BBB data (See Table S1 in the Supporting Information). According to P_e values previously described [34], compounds with P_e exceeding $4 \cdot 10^{-6}$ cm s^{-1} would be able to cross the BBB (cns+), whereas those displaying P_e less than $2 \cdot 10^{-6}$ cm s^{-1} would not reach the CNS (cns-) via passive diffusion. Between these two values the prediction is uncertain (cns +/-). While the asymmetric derivative *m*-**5b** with only one positive charge displayed an uncertain CNS penetration, the azocuronium salts with two positive charges, *m*-**1**(**a-d**) and *p*-**1**(**a**,**b**), were predicted not able to cross the BBB (Table 1).

Cytotoxicity of azocuroniums salts *m*-**1(a-d)**, *p*-**1(a,b)** and *m*-**5b** was determined in Raw 264.7 macrophages, using the quantitative colorimetric assay MTT (3-[4,5-dimethylthiazol-2-yl]-2,5-diphenyltetrazolium bromide) [41]. Compounds at a concentration of 10 μM were incubated with the cell line at 37 ºC during 24 h and then, the mitochondrial activity of living cells was measured by the absorbance change at 540 nm. All tested compounds showed cell viabilities in the same range than the basal experiment, pointing out that none of them showed any significant cytotoxic effect in this model.

As required for further development as potential therapeutic or research tools, we demonstrate that the new azocuronium salts *m*-**1(a-d)** and *p*-**1(a,b)** are soluble in

physiological medium, lack toxicity *in vitro* and are predicted to be CNS-impermeable via passive diffusion.

2.3. Photochemical characterization by UV/vis and ^{1}H-NMR

To study the photochemical behavior of new azocuroniums, we performed their spectroscopic characterization by UV/vis and ^{1}H-NMR.

UV/vis spectra of azocuroniums *m*-**1**(**a**-**d**), *p*-**1**(**a**,**b**) and *m*-**5b** were recorded in water at rt and the photochemical characterization of *m*-**1b** is given as an example (see Figure S1 in Supplementary Information for further details). The thermally equilibrated spectrum of *m*-**1b** (Figure 2B, black line) showed the two absorption bands characteristic of azobenzene derivatives. The most intense band maxima at 315 nm was assigned to the π-π^* electronic transition of the (*E*)-azobenzene moiety, while the other maxima around 425 nm is due to the forbidden n-π^* electronic transition. After irradiation with 335-340 nm light using a LED-based source (UV LED-light), the amplitude of the 315-nm band decreased along increasing irradiation time, while the amplitude of the 425-nm peak increased (red line). As previously reported, this spectral change is due to the (*E*)-to-(*Z*) isomerization of azobenzene molecules, which was reverted by irradiating with light of 400-450 nm (blue LED, blue line in Figure 2B) [14]. The insert in Figure 2B shows details of the UV/vis spectra between 375 nm and 525 nm.

To check the stability of new azocuroniums in the photoswitching process, we performed three consecutive cycles of interconversion, monitoring the absorption at 315 nm of *m*-**1b**

throughout alternating irradiation with blue LED and UV LED (Figure 2C). After each cycle, each species showed its characteristic absorption value namely, 0.54 AU for the (*E*)-isomer and 0.19 AU for the (*Z*)-form. Therefore, no evidence of photo-fatigue was observed under conditions close to functional studies in muscle-type nAChRs expressed in *Xenopus laevis* oocytes, where no more than two photoswitching cycles were used (see Section 2.5).

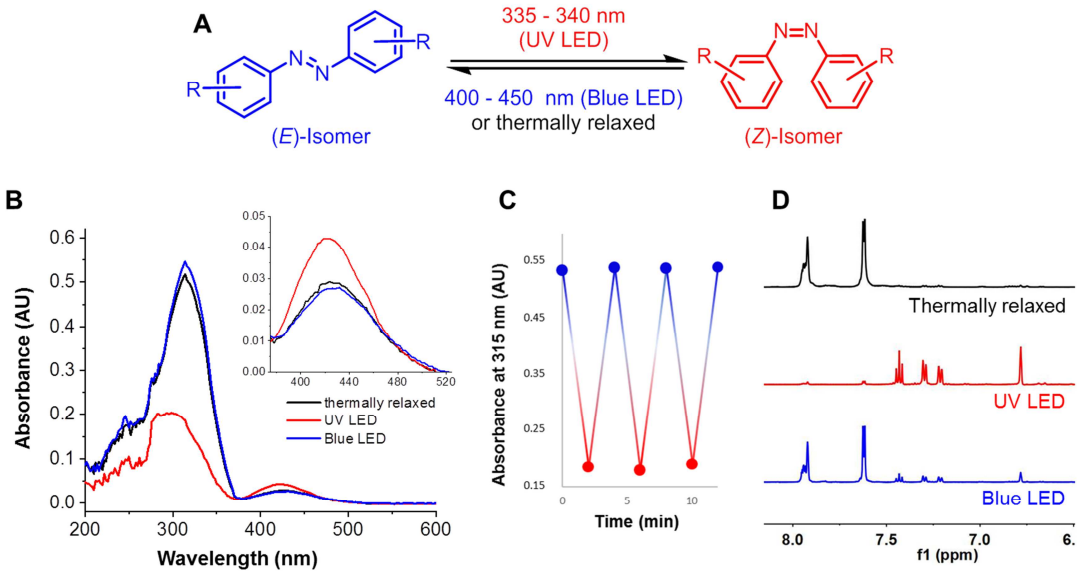

Figure 2. Photoswitched properties of *m*-**1b**. A) (*E*)-to-(*Z*) Isomerization of the azobenzene scaffold. B) UV/vis spectra of *m*-**1b** (50 μM) in water at rt, thermally relaxed (black line), irradiated with UV LED (red trace) and blue LED (blue trace). The inset shows a magnification of the n−π* band. C) Reversibility study of the photoisomerization of *m*-**1b** over three cycles, monitoring the absorption at 315 nm throughout alternating irradiation with blue LED (blue circle) and UV LED (red circle). D) Expansion of ^{1}H-NMR spectra of azocuronium *m*-**1b** at the indicated conditions.

The (*E*)-(*Z*) conversion of azocuroniums was also quantified by ^{1}H-NMR technique, using deuterium oxide (D_2O) as solvent. Solutions were irradiated under UV or blue LED-light into a round-bottom flask and then transferred to a NMR tube for registering ^{1}H-NMR spectra under darkness. The isomeric percentage was calculated from the integral of signals attributable to common protons in each species. The photo-induced (*E*)-to-(*Z*) isomerization of azocuroniums is more appreciable in the aromatic area, as explained below for *m*-**1b** (an expansion of this area is shown in Figure 2D). Firstly, the ^{1}H-NMR spectrum of the non-irradiated *m*-**1b** showed two groups of aromatic signals integrated for 8 protons, which were assigned to the (*E*)-azobenzene isomer (upper spectrum in Figure 2D). After LED irradiation under UV light at 335-340 nm, the photostationary state (PSS_{UV}) containing 96% of (*Z*)-isomer was reached (see Supplementary Information, page S23). Afterward, the solution was irradiated at 400-450 nm (blue LED) obtaining again the (*E*)-isomer in around 90% yield.

2.4. Radioligand binding assays at nAChRs

(*E*)-Azocuroniums *m*-**1**(**a**-**d**), *p*-**1**(**a**,**b**) and *m*-**5b** were assayed in human nicotinic receptors in radioligand-displacement experiments, using muscular nAChR and two neuronal-type nAChRs (α7 and α4β2) [42]. The radioligands used were [^{125}I]α-bungarotoxin (for muscle-type and α7 nAChRs) and [^{3}H]cytisine (for α4β2 nAChRs). The percentage of radioligand displacement of compounds at a single concentration (10 μM) was calculated for each receptor type and then, binding constants (K_i) were calculated for azocuroniums that produced a displacement percentage above 60%, using a range of 5 different concentrations

in 3 independent experiments (Table 2 and Figure S2 for further details). Standard reference compounds were α-bungarotoxin (muscle-type nAChR), epibatidine (α7 nAChR) and nicotine bitartrate (α4β2 nAChR), which were tested in each experiment at several concentrations to obtain competition curves, from which K_is were calculated.

Table 2. Binding constants at human nAChRs of muscular and neuronal-type (α7 and α4β2), or percentage of radioligand displacement (in brackets) at the specified concentration, of azocuroniums *m*-**1**(**a**-**d**), *p*-**1**(**a**,**b**) and *m*-**5b**.[a]

	K_i (nM)		
	Muscle-type	Neuronal α7	Neuronal α4β2
m-**1a**	42 ± 4	2500 ± 210	>10,000 (31%)
p-**1a**	200 ± 20	930 ± 80	>10,000 (45%)
m-**1b**	35 ± 3	910 ± 90	>10,000 (7%)
p-**1b**	1,100 ± 100	>10,000 (16%)	1,500 ± 130
m-**1c**	220 ± 20	1,900 ± 180	>10,000 (29%)
m-**1d**	100 ± 9	730 ± 70	>10,000 (32%)
m-**5b**	>10,000 (45%)	>10,000 (48%)	>10,000 (39%)
α-bungarotoxin	1.0 ± 0.1	n.d.	n.d.
epibatidine	n.d.	120 ± 10	n.d.
nicotine	n.d.	n.d.	1.5 ± 0.1

[a]Results are the mean ± SEM of three independent experiments. nd: not determined.

In general, *meta*-substitution in azocuronium salts favored the interactions with muscle-type nicotinic receptors ($K_i = 10^{-8}$ M) as compared to neuronal subtypes α7 ($K_i = 10^{-6} – 10^{-7}$ M) and α4β2 ($K_i > 10^{-5}$ M). Azocuroniums bearing *para*-substitutions were less active in all nAChRs and showed no selectivity towards the muscular type. For instance, the pyrrolidine derivative *p*-**1a** that was the most active *para*-azocuronium compound in muscular nAChR (K_i = 200 nM) showed α7-nAChR affinity in the same order of magnitude (K_i = 930 nM). Similarly, *para*-piperidine azocuronium *p*-**1b** was not selective either, this time between muscle-type and neuronal α4β2, as its binding constants were in the same range (K_i = 1,100 and 1,400 nM, respectively).

In muscle-type nAChRs, the most potent ligands were the *meta*-pyrrolidine *m*-**1a** and the *meta*-piperidine *m*-**1b** azocuroniums, with binding affinities in the nanomolar range (K_is = 42 nM and 35 nM, respectively). These ligands also showed a clear muscle-type selectivity as their affinities were in the micromolar range for α7 (K_is = 2,500 and 910 nM, respectively), and above in the case of α4β2 (K_is >10,000 nM). Thus, *m*-**1a** and *m*-**1b** displayed high binding affinity and selectivity ratios towards muscle-type nAChRs compared to the neuronal subtypes α7 (60- and 26-fold) and α4β2 (>240- and >290-fold).

Relative to the piperidine-substituted *m*-**1b**, both the ring expansion in the *meta*-azepane derivative *m*-**1c** or the introduction of a double bond to provide the *meta*-1,2,3,6-tetrahydropyridine derivative *m*-**1d**, decreased the binding affinity in muscle-type nAChR (K_is = 220 and 100 nM, respectively) and also diminished selectivity indexes between muscular and neuronal nAChRs. Finally, asymmetric derivative *m*-**5b** was poorly active in all nicotinic receptors assayed (Table 2), pointing out the importance of the presence of two cationic moieties for a successful nAChRs binding.

2.5. Functional characterization in nAChRs

We evaluated the effect of *meta*-azocuroniums in muscular nAChR expressed in *Xenopus laevis* oocytes. To activate nAChRs, a solution of ACh (50 μM, 2.3-18.4 nL) was delivered on the surface of the oocytes using a nano-injector (Figure 3A). This small volume of ACh ("puff") was washed out by perfusing the oocytes with a recirculating recording solution propelled by a pump attached to the chamber (Figure 3A). Above the oocyte, two LEDs were placed to drive photo-isomerization. These LEDs, hereafter referred to as "UV LED" and "blue LED", had their emission spectra centered at 335-340 nm and 400-450 nm, respectively. Receptor activity was assessed by measuring ionic currents through the plasma membrane mediated nAChR using the two-electrode voltage-clamp (TEVC) technique (Figure 3A). For current recordings, the membrane potential was held at -60 mV. Thus, nAChR activation will result in a downward deflection of the current trace, as the result of the net inward current through the receptors.

Under voltage-clamp, oocytes have a basal conductance, yielding relatively small background currents in the order of 0.05-0.2 μA. Oocytes displaying higher background currents were discarded. An ACh puff was applied after the recirculation pump was turned off. This allowed ACh to reach the membrane which activated nAChR, resulting in an increase of the membrane conductance (Figure 3B). Then, the pump was turned on, washing ACh from the oocyte's vicinity, deactivating nAChR. The deactivation of nAChR was made apparent by the decrease of the inward current amplitude (Figure 3B). Although the decay of the current amplitude was due to removal of ACh by activation of the pump, we cannot rule out the possibility that a small fraction of this is due to receptor desensitization. To address this we observed that with "no pumping" the decay of the

current was much slower (see Figure S3 in Supplementary Information), indicating that desensitization plays a minor role in our observations. Thus, we concluded that this approach allows us to evaluate the effect of the *meta*-azocuronium salts on muscular nAChRs.

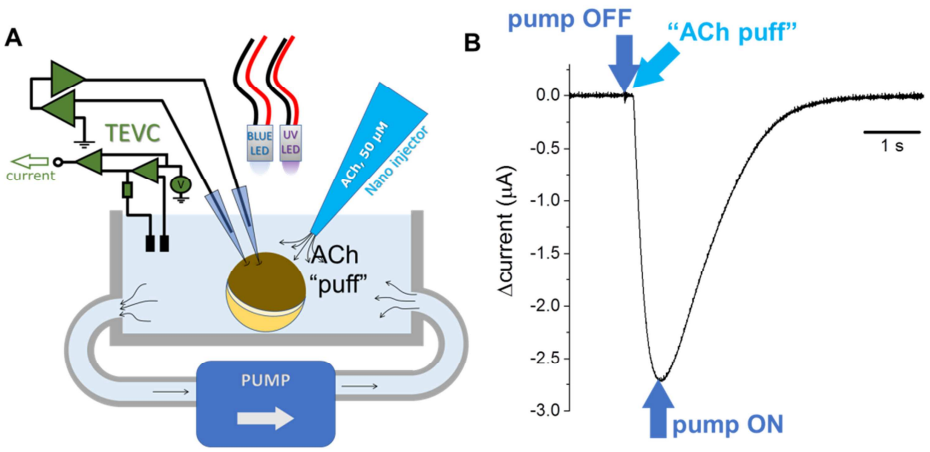

Figure 3. A) TEVC technique. Ionic currents were measured in *Xenopus* oocytes expressing embryonic mouse muscular nAChR. The membrane potential was held at –60 mV. Two LEDs (UV and blue) were used to drive isomerization, a nano-injector to deliver ACh (2.3-18.4 nL, 50 µM, 46 nL/s) on the surface of the oocytes, and a pump to circulate the solution and wash out ACh from oocytes. B) Record obtained by adding an ACh puff while the pump is turned off, as a control (no compound). The current increases due to the receptor activation.

*2.5.1. Piperidine-derived azocuronium salt m-**1b** blocks muscular nAChR*

Under voltage-clamp, inward currents were observed in oocytes expressing muscle-type nAChR upon application of an ACh puff (Figure 4A, green trace). This response was inhibited by the addition of the *meta*-piperidine azocuronium *m*-**1b** (5 µM) to the recording

solution. Such inhibition was observed by a decrease in the maximum amplitude of the currents (Figure 4A, black trace). The inhibitory effect of *m*-**1b** on current amplitude was partially reverted when oocytes and the surrounding solution were irradiated with the UV LED for 5 minutes before applying a ACh puff and during the recording (Figure 4A, red trace). The inhibitory effect of *m*-**1b** was recovered by irradiating with the blue LED. These observations suggested that *m*-**1b** acted on the deactivated (closed) receptors.

To understand whether compound *m*-**1b** could act on activated (open) receptors, nAChR currents were recorded in the presence of *m*-**1b** (0.5 μM) which was held in its (*Z*)-isomer by constant irradiation with the UV LED. We performed this assay with no perfusion to prolong the activating effect of ACh on the receptor. Following nAChR activation and blue LED irradiation [(*E*)-isomer], a faster decay of the ACh-induced current was observed (Figure 4B, red trace) with respect to the case when constant UV radiation was applied (Figure 4B, black trace). Since the perfusion pump was switched off, the decay observed during constant UV LED was likely due to receptor desensitization. Swapping the UV LED for the blue LED radiation [(*E*)-isomer] caused a faster decrease in the current amplitude (Figure 4B, red trace), indicating that *m*-**1b** was like affecting receptors in any isomeric form.

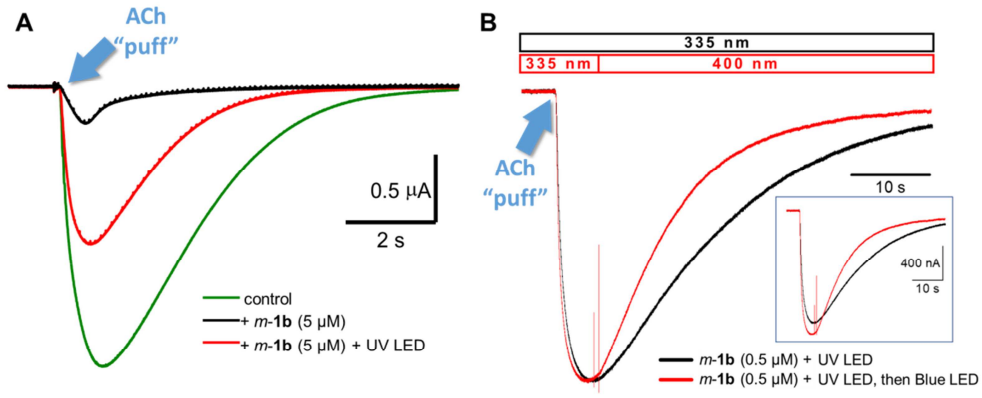

Figure 4. Effects of *m*-**1b** in the electrical signal at indicated conditions. A) A "puff" of ACh (green trace) evoked currents in oocytes that decreased after adding (*E*)-*m*-**1b**, showing an almost complete inhibition of the receptors (black trace). After that, UV LED lighting [(*Z*)-isomer] partially reversed the effect of (*E*)-isomer (red trace). B) Currents evoked by the (*Z*)-isomer (black trace); exchange the UV LED for the blue LED radiation [(*E*)-isomer] caused a faster decrease in the current amplitude (red trace).

To further characterize the action of *m*-**1b** on nAChR, we evaluate the relationship between drug concentration and receptor inhibition. For this purpose, we performed recordings of ACh activity in the presence of the thermally relaxed *m*-**1b** [(*E*)-isomer]. As the concentration of *m*-**1b** increased, the response to ACh puff decreased (Figure 5A, left). This inhibitory effect was partially reverted upon irradiation with UV LED for 5 minutes [(*Z*)-isomer] (Figure 5A, right). To assess the inhibitory effect of *m*-**1b** in detail, we performed recordings in the presence of a range of concentrations of *m*-**1b** (0.05-20 µM) thermally relaxed [(*E*)-isomer] (Figure 5B, black trace) and after UV radiation [(*Z*)-isomer] (Figure 5B, red trace) and we plotted the average of current amplitude normalized with respect to

recording in the absence of the drug. The current-*vs*-dose plots were fitted to a simple one-site binding model, yielding an apparent half-maximum inhibitory constant (K_i) of 0.46 ± 0.06 μM (n = 24) for the thermally relaxed *m*-**1b** (Figure 5B, black trace) and 2.6 ± 0.5 μM (n = 24) for the UV-irradiated *m*-**1b** (Figure 5B, red trace).

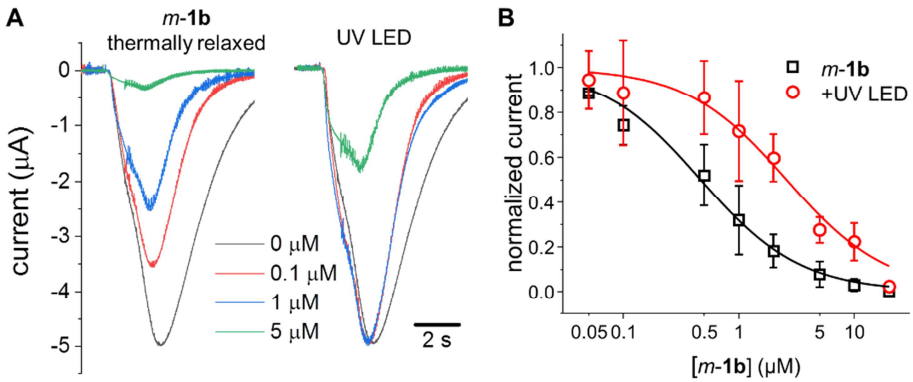

Figure 5. Compound *m*-**1b** is a light-dependent antagonist. A) AChR currents recorded upon application of an ACh "puff" (50 μM, 9.2 nL) in the absence (black trace) and presence of 0-5 μM *m*-**1b** thermally relaxed (left) or while irradiating with the UV LED. B) The maximum amplitude of the currents was normalized with respect to the maximal amplitude observed in the absence of *m*-**1b** when it was thermally relaxed (black symbols) or after irradiation at 340 nm (red symbols).

We noticed that the variability in current amplitude for the UV-irradiated drugs was slightly higher than for their thermally relaxed counterparts. Although we consider this issue to be beyond the scope of the present study, we argue that such increase in variability could be

attributed to variations in the effective intensities of the UV radiation that reached oocytes. We did not evaluate this issue systematically, yet we noticed that it depended on the angle of the incidence of the LED beam and the recording chamber. For this reason, we opted to skip to further analyzing the (*E*)-to-(*Z*) isomerization time course for this study.

*2.5.2. Pyrrolidine-based azocuronium salt m-**1a** acts as a muscular nAChR agonist*

Next, we proceed to evaluate the compound *m*-**1a** which differed from *m*-**1b** on the smaller ring size of the quaternary amine. We observed that exposing the oocytes to thermally relaxed *m*-**1a** [(*E*)-isomer] produced the activation of the nAChR current and thus, we proceeded with a different approach. Voltage-clamped oocytes were exposed to *m*-**1a** under constant UV irradiation to keep the compound as (*Z*)-isomer. To test the effect of the (*E*)-isomer, a 5-second pulse of blue radiation was applied while turning off the UV LED. After 5 seconds, the UV LED was turned back on [(*Z*)-isomer]. Turning on the blue LED activated nAChRs, as a robust inwards current was detected (Figure 6A). This agonist behavior was observed at different concentrations of *m*-**1a**, ranging from 0.5 to 10 μM. Activation of the current showed a clear concentration dependence, with an apparent half-maximum activity constant of 4.2 ± 0.4 μM (n = 4) (Figure 6B).

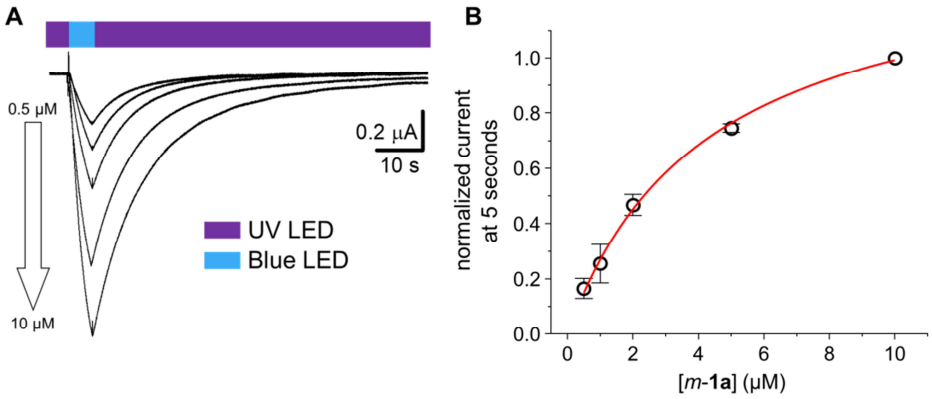

Figure 6. Azocuronium *m*-**1a** is a light-dependent agonist of the nAChR. A) Current recordings in the presence of 0.5-10 µM *m*-**1a**. Constant irradiation with the UV LED made *m*-**1a** inactive as agonist. Inducing the isomerization to the (*E*)-isomer with a 5-second pulse of blue LED resulted in a robust increase of the nAChR current. This activation was readily reverted by turning back to irradiation with the UV LED. B) Average normalized current measure following 5 seconds of activation showed a clear concentration-dependence for activation.

Per our initial hypothesis, the hydrophobic character of the molecule's quaternary amine seems to determine whether the agonist/antagonist activity profile. To this point, the piperidine-based *m*-**1b** functions as an antagonist of nAChR, while the pyrrolidine-based *m*-**1a** behaves as an agonist.

*2.5.3. Azepane-derived azocuronium salt m-**1c** behaves as a muscular nAChR antagonist*

The compound *m*-**1c** bears a larger hydrophobic moiety (azepane fragment) associated to the quaternary amine. Consistent with our initial hypothesis, *m*-**1c** inhibited ACh-induced current in oocytes expressing nAChRs. Fitting the normalized current-*vs*-dose plots to a one-site binding model for the thermally relaxed *m*-**1c** [(*E*)-isomer] yielded a K_i of 0.33 ± 0.04 μM (n = 26) (not shown). However, the plot for the UV-irradiated drug was not properly fitted to the one-site model, leading us to consider the fact that muscular nAChR have two distinct ACh binding sites with different pharmacology. Therefore, we chose to fit plots to a Hill equation, from which we calculated K_is of 0.30 ± 0.02 μM and 2.6 ± 0.5 μM for the (*E*) and (*Z*)-isomer, respectively (Figure 7). As expected, the Hill coefficient for the thermally relaxed *m*-**1c** was near one (0.97 ± 0.05), consistent with the previous fit. In the case of the UV-irradiated *m*-**1c**, the Hill coefficient was 0.56 ± 0.07. It is well-known that ACh binding and activation of the muscular nAChR is highly cooperative, where the binding of one ACh leads to an increase in affinity for the second ACh molecule [9,43]. Based on this we speculate that, assuming that *m*-**1c** binds to the ACh sites, the interaction of *m*-**1c** on one site induces a reduction of the affinity of the other site for this drug. Since both sites are allosterically coupled, we speculate that there were at least two *m*-**1c** molecules bound to each nAChR, with the first molecule inducing a conformational change that leads to a decrease in the affinity of the receptor for the second one. Accordingly, we speculate that the (*E*)-isomer of *m*-**1c** (and *m*-**1b**) to occupy one of the ACh binding sites, hindering further steps in the activation of the receptor. However, the (*Z*)-isomer of *m*-**1c** seems to be competed out by ACh so that the binding of ACh allosterically decreases the affinity of the receptor for *m*-**1c**. Notwithstanding the importance of determine the

underlying process, pinpointing the mechanism responsible for this reduction in the Hill coefficient was beyond the scope of this study.

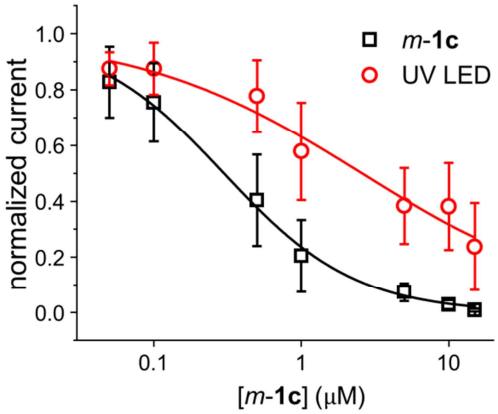

Figure 7. Inhibition of nAChR current by *m*-**1c** when thermally relaxed (black squares) and under irradiation with UV LED (red circles). The current-*vs*-[*m*-**1c**] plots were fitted to a Hill equation, yielding a K_i value of 0.30 ± 0.02 μM and 2.6 ± 0.5 μM, respectively. The corresponding Hill coefficients were 0.97 ± 0.05 and 0.56 ± 0.07 (n = 26).

2.5.4. The rigidity of the N-cycle is important for activity

Next, we explored the effect of the rigidity of the *N*-cycle on the action of the drug. For this purpose, we used piperidine derivative *m*-**1b** as reference and compared it to the double-bond bearing piperidine compound *m*-**1d**. The latter *N*-cycle has less flexible, more planar geometry than the one of *m*-**1b**. Like this reference compound, *m*-**1d** behaved as an antagonist of nAChR. Both the thermal relaxed and UV-irradiated *m*-**1d** showed very similar K_i values of 0.84 ± 0.09 μM and 0.88 ± 0.11 μM (n = 15), respectively (Figure 8).

In spite of the similarity in the receptor's affinity for both isomers, the efficacy for drug action was isomer-dependent. Per the fitting analysis, the fractions of active receptors at saturating concentration of *m*-**1d** were 0.11 ± 0.04 and 0.35 ± 0.03 for the thermally relaxed and UV-irradiated *m*-**1d**, respectively. This indicated that this drug was likely operating with a distinct mechanism that those ones described above. Furthermore, it is noteworthy, that Hill coefficients fitted for both isomers were similar, 3.5 ± 1.3 and 2.9 ± 1.1, and higher than those of the drugs tested here. These values indicated that a highly cooperative process underlies the inhibition by *m*-**1d**. Understanding the nature of this process was beyond the scope of this study.

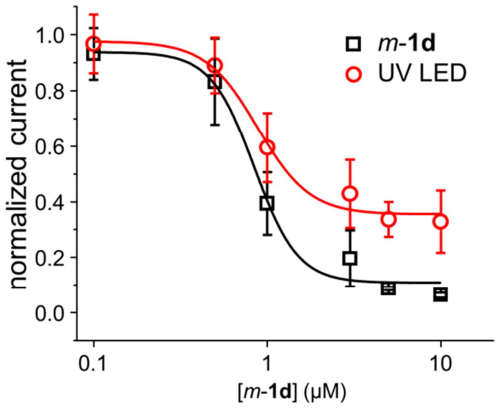

Figure 8. Inhibition of nAChR current by thermally relaxed *m*-**1d** (black squares) and under irradiation with UV LED (red circles). Fitting to a Hill equation, yielded a K_i of 0.84 ± 0.09 μM and 0.88 ± 0.11 μM, respectively. The current fraction at maximum inhibition was 0.11 ± 0.04 and 0.35 ± 0.03 for the thermal relaxed and UV-irradiated *m*-**1d**, respectively. The corresponding Hill coefficients were 3.5 ± 1.3 and 2.9 ± 1.1 (n = 15).

3. Conclusions

Azocuroniums were designed by adding two *N*-methyl-*N*-carbocyclic quaternary ammonium groups to an azobenzene scaffold in *meta*- or *para*-position. These new photoswitchable compounds showed good solubility in physiologic media, negligible toxicity *in vitro* and as expected, they would not penetrate into the CNS. They can be easily photoisomerized between the (*E*)- and (*Z*)-forms by irradiation at 400-450 nm (blue LED) and 335-340 nm (UV-LED), respectively.

In radioligand binding assays at nAChRs, *meta*-substituted azocuroniums were more potent and selective towards neuromuscular receptors than their *para*-substituted counterparts. Derivatives with smaller cationic heads, namely the *meta*-pyrrolidine *m*-**1a** and the *meta*-piperidine *m*-**1b** azocuroniums emerged as the most potent and selective ligands in muscle-type nAChRs, with binding affinities in the nanomolar range (K_is = 42 nM and 35 nM, respectively). Moreover, they presented lower affinities for α7 (K_is = 2,500 and 910 nM, respectively) and were almost inactive in α4β2 (K_is >10,000 nM), showing interesting subtype selectivity. In contrast, azocuroniums with increased volume or rigidity in the *N*-carbocycle, namely the *meta*-azepane and the *meta*-1,2,3,6-tetrahydropyridine derivatives (*m*-**1c** and *m*-**1d**), showed reduced binding constants in muscular-type nAChR (K_is = 220 and 100 nM, respectively) with diminished selectivity indexes between muscular and neuronal nAChRs.

Using the two-electrode voltage-clamp technique, we evaluated the functional activity of *meta*-azocuroniums *m*-**1(a-d)** in muscular nAChR expressed in *Xenopus laevis* oocytes. By irradiation with blue-LED or UV-LED while recording electrical currents, in all cases the

(*E*)-conformation was found to be more potent than the corresponding (*Z*)-isomer. The volume and hydrophobic character of the ammonium groups seemed to determine whether these azocuronium salts would block or activate the receptor. All *meta*-azocuroniums behaved as antagonists of muscular nAChR, with the exception of the smallest pyrrolidine derivative *m*-**1a**. When *m*-**1a** was constantly irradiated with blue LED to obtain the (*E*)-isomer, a robust increase of the nAChR current was observed in a concentration-dependent manner, giving an apparent half-maximum binding constant of 4.2 ± 0.4 μM. (*E*)-Isomer of azocuronium salts derived from piperidine (*m*-**1b**), azepane (*m*-**1c**) or 1,2,3,6-tetrahydropyridine (*m*-**1d**) behaved as antagonists of muscular nAChR and retained greater activity than their (*Z*)-isomer counterparts.

The selectivity, photoswitchable properties, synthetic accessibility along with the ability to control their qualitative effect via modification of the quaternary ammonium residues makes this family of compounds interesting tools to better understand the dynamics of activation and blockade of muscular nAChRs and potential candidates for the development of light-targeted muscle relaxants.

4. Experimental section

4.1. Chemistry. General methods

High-grade reagents and solvents were purchased from common commercial suppliers, mostly Sigma-Aldrich, and were used without further purification. Reactions were followed either by analytical thin-layer chromatography (TLC) or by high-performance liquid chromatography – mass spectrometry (HPLC-MS). TLC were carried out on Merck silica gel 60 F254 plates, by visualization with UV-light (λ = 254 or 365 nm) and/or by staining with ninhydrin solution in ethanol. HPLC-MS were performed on an analytical Waters equip (Alliance Watters 2695) composed of a SunFire C_{18} (3.5 μm, 4.6 mm x 50 mm) column and a UV-visible photodiode array detector (λ = 190-700 nm) coupled to a quadrupole mass spectrometer (Micromass ZQ). Spectra were acquired in an electrospray ionization (ESI) interface working in the positive or negative-ion mode. Reactions under mw irradiation were performed in a Biotage Initiator 2.5 reactor. Products were purified by preparative TLC on Merck silica gel 60 F254 plates or crystallization. HPLC analyses were used to confirm the purity of all compounds (≥ 95%) and were performed on Waters 2690 equipment, at a flow rate of 1.0 mL/min, with a UV-visible photodiode array detector (λ = 190 - 700 nm), using SunFire C_{18} (3.5 μm, 4.6 mm x 50 mm) column. The gradient mobile phase consisted of H_2O:ACN with 0.1% formic acid as solvent modifiers, the gradients time (g.t.) and the retention time (t_R) are indicated for each compound. Melting points (mp, uncorrected) were determined in a MP70 apparatus (Mettler Toledo). Nuclear magnetic resonance (^{1}H NMR and ^{13}C NMR) spectra were obtained in CD_3OD, DMSO-d_6, $CDCl_3$ or D_2O solutions using the following NMR spectrometers: Varian INOVA-300, Varian

INOVA-400, Varian Mercury-400 or Varian Unity-500. Chemical shifts (δ) are reported in parts per million (ppm) relatives to internal tetramethylsilane scale (δ_H 00). In the case of D_2O solutions, ^{13}C shifts were determined relative to 1,4-dioxane (δ_C 67.19). Coupling constants (*J*) are described in hertz (Hz). 2D NMR experiments – homonuclear correlation spectroscopy (H, H-COSY), heteronuclear multiple quantum correlation (HMQC) and heteronuclear multiple bond correlation (HMBC) – of representative compounds were acquired to assign protons and carbons of new structures. The high-resolution mass spectra (HRMS) were carried out by using an Agilent 1200 Series LC system (equipped with a binary pump, an auto sampler, and a column oven) coupled to a 6520 quadrupole-time of flight (QTOF) mass spectrometer. ACN:H_2O (75:25, v:v) was used as mobile phase at 0.2 mL/min. The ionization source was an ESI interface working in the positive-ion mode. The electrospray voltage was set at 4.5 kV, the fragmentor voltage at 150 V and the drying gas temperature at 300 °C. Nitrogen (99.5% purity) was used as nebulizer (207 kPa) and drying gas (6 mL/min).

*4.2. General procedure for the synthesis of nitro derivatives m-**2(a-d)** and p-**2(a,b)***

The appropriate amine (1 equiv.) and K_2CO_3 (1.2 equiv.) in dry acetone (7 mL/mmol) was stirred 10 min at rt. Then, benzyl bromide (1 equiv.) was added and the mixture was heated at 120 ºC under mw irradiation for 10 min. The solvent was evaporated under reduced pressure. EtOAc was added and the organic phase washed with H_2O and brine, dried ($MgSO_4$), filtered, and evaporated under reduced pressure. Nitro derivatives were obtained and used without further purification. With the exception of *m*-**2d**, the rest of these

intermediates were previously described (*m*-**2a** [44], *p*-**2a** [45], *m*-**2b** [46], *p*-**2b** [47], *m*-**2c** [48]).

*4.2.1. 1-[(3-Nitrophenyl)methyl]-1,2,3,6-tetrahydropyridine (m-**2d**)*

Yellow-brown solid (quantitative yield) of mp 90-93 ºC. ^{1}H NMR (400 MHz, $CDCl_3$): δ 8.22 (bs, 1H, H_o), 8.11 (d, *J* = 8.2 Hz, 1H, H_p), 7.71 (d, *J* = 7.6 Hz, 1H, $H_{o'}$), 7.48 (t, *J* = 7.9 Hz, 1H, $H_{m'}$), 5.80-5.74 (m, 1H, H_4), 5.69-5.63 (m, 1H, H_3), 3.66 (s, 2H, H_α), 3.02- 2.96 (m, 2H, H_2), 2.57 (t, *J* = 5.7 Hz, 2H, H_6), 2.20-2.15 (m, 2H, H_5). ^{13}C NMR (101 MHz, $CDCl_3$): δ 148.5 (C_m), 141.2 (C_i), 135.1 ($C_{o'}$), 129.3 ($C_{m'}$), 125.4 (C_4), 125.2 (C_3), 123.9 (C_o), 122.3 (C_p), 62.1 (C_α), 52.9 (C_2), 49.9 (C_6), 26.2 (C_5). HPLC-MS (2:30- g.t.5 min) t_R 1.47 min, *m/z* = 219.28 $[M+H]^+$.

*4.3. General procedure for the synthesis of symmetric azobenzene derivatives m-**3(a-d)** and p-**3(a,b)***

A solution of $LiAlH_4$ in Et_2O (1M or 2M, 5 equiv.) was added dropwise to the stirred solution of a nitro derivative *m*-**2**(**a**-**d**) or *p*-**2**(**a**,**b**) (1 equiv.) in dry Et_2O at -78 ºC. After 15 min, the mixture was allowed to warm to rt and then stirred overnight. The excess of $LiAlH_4$ was carefully quenched with H_2O. The reaction mixture was filtered and washed with cold H_2O several times. The mixture was acidified with a solution of citric acid (10%) and the organic phase was separated and evaporated under reduced pressure. The residue was purified by preparative TLC in the corresponding gradient.

*4.3.1. 1,2-Bis[3-(pyrrolidin-1-ylmethyl)phenyl]diazene (m-**3a**)*

Following the general procedure, from nitro derivative *m*-**2a** (159 mg, 0.77 mmol) and $LiAlH_4$ (1.93 mL, 3.85 mmol) diazene *m*-**3a** was prepared. After a purification by TLC (EtOAc:MeOH, 90:10), a mixture of (*E*):(*Z*)-isomers (ca. 80:20) of *m*-**3a** was obtained as orange crystals (121 mg, 90% yield) of mp 62-64 ºC. ^{1}H NMR (500 MHz, CD_3OD) (*E*)-Isomer: δ 7.92 (s, 2H, H_o), 7.86 – 7.83 (m, 2H, $H_{o'}$), 7.55 – 7.50 (m, 4H, $H_{m'}$, H_p), 3.76 (s, 4H, H_α), 2.62 – 2.57 (m, 8H, H_2), 1.84 (tt, *J* = 3.8, 1.9 Hz, 8H, H_3); (*Z*)-Isomer: δ 7.29 (t, *J* = 7.8 Hz, 2H, $H_{m'}$), 7.14 (dt, *J* = 6.6, 1.0 Hz, 2H, H_p), 6.88 (d, *J* = 7.9 Hz, 2H, $H_{o'}$), 6.72 (s, 2H, H_o), 3.49 (s, 4H, H_α), 2.32 – 2.30 (m, 8H, H_2), 1.74 – 1.71 (m, 8H, H_3). ^{13}C NMR (126 MHz, CD_3OD) (*E*)-Isomer: δ 154.1 (C_i), 140.9 (C_m), 133.2 (C_p), 130.3 ($C_{m'}$), 124.4 (C_o), 123.10 ($C_{o'}$), 61.15 (C_α), 54.98 (C_2), 24.15 (C_3). (*Z*)-Isomer: δ 155.3 (C_i), 140.3 (C_m), 130.0 (C_p), 129.3 ($C_{m'}$), 121.60 (C_o), 121.03 ($C_{o'}$), 60.70 (C_α), 54.62 (C_2), 24.04 (C_3). HPLC-MS (2:30 - g.t. 10 min) t_R 5.96 min, m/z = 349.47 $[M+H]^+$. HRMS [ESI+] m/z = 348.23092 [M], calcd for $[C_{22}H_{28}N_4]$ 348.2314.

*4.3.2. 1,2-Bis[4-(pyrrolidin-1-ylmethyl)phenyl]diazene (p-**3a**)*

Diazene *p*-**3a** was prepared from nitro derivative *p*-**2a** (138 mg, 0.67 mmol) and $LiAlH_4$ (1.67 mL, 3.34 mmol) following the general procedure. After a preparative TLC using EtOAc:MeOH (95:5) as eluent, compound *p*-**3a** was obtained (brown oil, 108 mg, 93%) as a mixture of (*E*):(*Z*)-isomers in proportion 95:5. ^{1}H NMR (500 MHz, CD_3OD) (*E*)-Isomer: δ 8.27 (d, *J* = 8.4 Hz, 4H, H_o), 7.92 (d, *J* = 8.4 Hz, 4H, H_m), 4.12 (s, 4H, H_α), 2.99 (m, 8H, H_2), 2.25 – 2.20 (m, 8H, H_3). (*Z*)-Isomer: δ 7.65 (d, *J* = 8.3 Hz, 4H, H_o), 7.21 (d, *J* = 8.3 Hz,

4H, H_m) 3.57 (s, 4H, H_α), 2.51 – 2.47 (m, 8H, H_2), 1.80 – 1.77 (m, 8H, H_3). ^{13}C NMR (126 MHz, CD_3OD) (*E*)-Isomer: δ 153.3 (C_i), 143.0 (C_p), 131.2 (C_m), 123.8 (C_o), 61.06 (C_α), 55.0 (C_2), 24.2 (C_3). HPLC-MS (2:30 - g.t.10 min) t_R 6.22 min, m/z = 349.21 $[M+H]^+$. HRMS [ESI+] m/z = 348.23157 [M], calcd for $[C_{22}H_{28}N_4]$ 348.2314.

*4.3.3. 1,2-Bis[3-(piperidin-1-ylmethyl)phenyl]diazene (m-**3b**)*

Diazene *m*-**3b** was obtained from nitro *m*-**2b** (150 mg, 0.68 mmol) and $LiAlH_4$ (3.41 mL, 3.41 mmol) following the general procedure, as orange crystals (124 mg, 97%) of mp 89-92 ºC. Purification by preparative TLC (EtOAc:MeOH 90:10). ^{1}H NMR (500 MHz, CD_3OD) mixture of isomers (*E*):(*Z*) (75:25), δ 7.93 - 7.89 (bs, 2H, H_o *E*), 7.85 (dt, *J* = 7.3, 1.9 Hz, 2H, $H_{o'}$, *E*), 7.52 (t, *J* = 5 Hz, 2H, $H_{m'}$, *E*), 7.50 (dt, *J* = 10, 2 Hz, 2H, H_p, *E*), 7.30 (t, *J* = 7.7 Hz, 2H, $H_{m'}$, *Z*), 7.13 (ddd, *J* = 7.6, 1.7, 1.1 Hz, 2H, $H_{o'}$, *Z*), 6.94 (ddd, *J* = 7.9, 2.1, 1.1 Hz, 2H, H_p, *Z*), 6.64 (m, 2H, H_o, *Z*), 3.63 (s, 4H, H_α,*E*), 3.35 (s, 4H, H_α, *Z*), 2.49 (s, 8H, H_2), 1.63 (p, *J* = 5.7 Hz, 8H, H_3), 1.50 (m, 4H, H_4). ^{13}C NMR (126 MHz, CD_3OD) (*E*)-Isomer: δ 154.0 (C_i), 133.7 (C_m), 130.2 ($C_{m'}$), 124.9 (C_p), 123.1 (C_o), 121.8 ($C_{o'}$), 64.4 (C_α), 55.4 (C_2), 26.5 (C_3), 25.2 (C_4). HPLC-MS (2:30 - g.t.10 min) t_R 6.22 min, m/z = 377.47 $[M+H]^+$.

*4.3.4. 1,2-Bis[4-(piperidin-1-ylmethyl)phenyl]diazene (p-**3b**)*

Following the general procedure, from nitro derivative *p*-**2b** (150 mg, 0.68 mmol) and $LiAlH_4$ (1M, 3.41 mL, 3.41 mmol) diazene *p*-**3b** was prepared. After a purification by TLC (EtOAc:MeOH, 95:5), a mixture of (*E*):(*Z*)-isomers (ca. 90:10) of *p*-**3b** was obtained as

orange crystals (122 mg, 95% yield) of mp 141-142 ºC. In ^{1}H and ^{13}C-NMR only picks of the (*E*)-isomer have been characterized. ^{1}H NMR (300 MHz, CD_3OD): δ 7.88 (d, *J* = 8.3 Hz, 4H, H_o), 7.52 (d, *J* = 8.2 Hz, 4H, H_m), 3.58 (s, 4H, H_α), 2.47 (s, 8H, H_2), 1.62 (s, 8H, H_3), 1.48 (s, 4H, H_4). ^{13}C NMR (75 MHz, CD_3OD): δ 153.3 (C_i), 139.9 (C_p), 131.6 (C_m), 123.6 (C_o), 64.3 (C_α), 55.5 (C_2), 26.6 (C_3), 25.2 (C_4). HPLC-MS (2:30 - g.t.10 min) t_R 6.15 min, m/z = 377.18 $[M+H]^+$.

*4.3.5. 1,2-Bis[3-(azepan-1-ylmethyl)phenyl]diazene (m-**3c**)*

Diazene *m*-**3c** was prepared from nitro *m*-**2c** (540 mg, 2.31 mmol) and $LiAlH_4$ (1M, 11.55 mL, 11.55 mmol) following the general procedure. After a preparative TLC using EtOAc:MeOH (70:30) as eluent, (*E*)-*m*-**3c** was obtained as an orange oil (283 mg, 61 %), with an isomeric purity >99%. ^{1}H NMR (500 MHz, DMSO): δ 7.84 (s, 2H, H_o), 7.76 (dt, *J* = 7.1, 2.0 Hz, 2H, $H_{o'}$), 7.55 (t, *J* = 7.5 Hz, 2H, $H_{m'}$), 7.53 – 7.50 (m, 2H, H_p), 3.73 (s, 4H, H_α), 2.63 – 2.59 (m, 8H, H_2, H_7), 1.65 – 1.54 (m, 16H, H_3, H_4, H_5, H_6). ^{13}C NMR (126 MHz, DMSO): δ 152.0 (C_i), 141.5 (C_m), 131.5 (C_p), 129.2 ($C_{m'}$), 122.1 (C_o), 121.3 ($C_{o'}$), 61.4 (C_α), 55.0 (C_2, C_7), 27.9 (CH_2), 26.5 (CH_2). HPLC-MS (2:30- g.t.10 min) t_R 9.66 min, *m/z* = 405.38 $[M+H]^+$, λ_{max} = 320 nm [(*E*)-isomer]. HRMS [ESI^+] m/z = 404.29324 $[M]^+$, calcd for $[C_{26}H_{36}N_4]^+$ 404.2940.

*4.3.6. 1,2-Bis{3-[(3,6-dihydropyridin-1(2H)-yl)methyl]phenyl}diazene (m-**3d**)*

From nitro derivative *m*-**2d** (300 mg, 1.37 mmol) and $LiAlH_4$ (1M, 6.87 mL, 6.87 mmol) compound *m*-**3d** was prepared. After a preparative TLC using EtOAc:MeOH (95:5) as eluent, a mixture of (*E*):(*Z*)-isomers (ca. 90:10) of diazene *m*-**3d** was obtained as orange crystals (126 mg, 49%) of mp 90-93 ºC. ^{1}H NMR (500 MHz, $CDCl_3$) (*E*)-Isomer: δ 7.89 (t, *J* = 1.9 Hz, 2H, H_o), 7.81 (dt, *J* = 7.5, 1.7 Hz, 2H, $H_{o'}$), 7.50 (dt, *J* = 7.6, 1.6 Hz, 2H, H_p), 7.46 (t, *J* = 7.6 Hz, 2H, $H_{m'}$), 5.77 (dtt, *J* = 9.4, 3.7, 2.1 Hz, 2H, H_4), 5.68 (dtt, *J* = 10.1, 3.3, 1.8 Hz, 2H, H_3), 3.68 (s, 4H, H_α), 3.02 (p, *J* = 2.8 Hz, 4H, H_2), 2.61 (t, *J* = 5.7 Hz, 4H, H_6), 2.19 (tp, *J* = 5.7, 2.8 Hz, 4H, H_5). (*Z*)-Isomer: δ 7.21 (t, *J* = 7.7 Hz, 2H, $H_{m'}$), 7.12 (d, *J* = 7.7 Hz, 2H, H_p), 6.83 (dt, *J* = 7.9, 1.5 Hz, 2H, $H_{o'}$), 6.72 (s, 2H, H_o), 5.73 – 5.70 (m, 2H, =CH) 5.58 (dtd, *J* = 10.0, 3.4, 1.7 Hz, 2H, =CH), 3.42 (s, 4H, H_α), 2.75 (dt, *J* = 5.3, 2.6 Hz, 4H, H_2), 2.35 (t, *J* = 5.7 Hz, 4H, H_6), 2.06 (dt, *J* = 5.7, 2.8 Hz, 4H, H_5). ^{13}C NMR (126 MHz, $CDCl_3$) (*E*)-Isomer: δ 152.9 (C_i), 139.8 (C_m), 131.8 (C_p), 129.1 ($C_{m'}$), 125.5 (C_4), 125.4 (C_3), 123.6 (C_o), 121.8 ($C_{o'}$), 62.8 (C_α), 53.0 (C_2), 49.9 (C_6), 26.3 (C_5). (*Z*)-Isomer: δ 154.7 (C_i), 139.3 (C_m), 128.7 ($C_{m'}$), 128.0 (C_p), 125.3 (2 =CH), 120.7 (C_o), 119.8 ($C_{o'}$), 62.5 (C_α), 52.6 (C_2), 49.6 (C_6), 26.2 (C_5). HPLC-MS (2:30- g.t.10 min) t_R 7.63 min, *m/z* = 373.28 $[M+H]^+$. λ_{max} = 319 nm [(*E*)-isomer]. HRMS [ESI^+] m/z = 372.23053 $[M]^+$, calcd for $[C_{24}H_{28}N_4]^+$ 372.2314.

*4.3.7. 1-[3-(Phenyldiazenyl)benzyl]piperidine (m-**4b**)*

To a solution of commercial nitrosobenzene (100 mg, 0.93 mmol) in anhydrous toluene (5 mL), 3-(piperidin-1-ylmethyl)aniline (178 mg, 0.93 mmol) and acetic acid (21 µL, 3.75

mmol) were added orderly under N_2 and the reaction was stirred at 60 ºC overnight. The mixture was extracted with EtOAc, washed with water and brine, dried with $MgSO_4$, filtered and concentrated under reduced pressure. The residue was purified in reverse phase flash column, from H_2O to ACN. After lyophilization of the appropriate fractions diazene *m*-**4b** was obtained as orange oil (241 mg, 93% yield), with an (*E*)-isomeric purity >99%. ^{1}H NMR (500 MHz, DMSO): δ 7.90 (dd, *J* = 6.6, 1.5 Hz, 2H, $H_{m''}$), 7.80 (t, *J* = 1.5 Hz, 1H, H_o), 7.78 (dt, *J* = 7.7, 1.8 Hz, 1H, $H_{o'}$), 7.63 – 7.57 (m, 3H, $H_{o''}$, $H_{p'}$), 7.54 (t, *J* = 7.6 Hz, 1H, $H_{m'}$), 7.49 (dt, *J* = 7.6, 1.4 Hz, 1H, H_p), 3.53 (s, 2H, H_α), 2.39 – 2.31 (m, 4H, H_2, H_6), 1.50 (p, *J* = 5.6 Hz, 4H, H_3, H_5), 1.40 (q, *J* = 6.0 Hz, 2H, H_4). ^{13}C NMR (126 MHz, DMSO): δ 152.0 ($C_{i'}$), 151.9 (C_i), 140.4 (C_m), 131.9 (C_p), 131.5 ($C_{p'}$), 129.5 ($C_{o''}$), 129.3 ($C_{m'}$), 122.5 ($C_{m''}$), 122.4 (C_o), 121.5 ($C_{o'}$), 62.4 (C_α), 53.9 (C_2), 25.6 (C_3), 24.0 (C_4). HPLC-MS (15:95-g.t.10 min) t_R 1.44 min, *m/z* = 280.28 $[M+H]^+$ (*Z*)-isomer; 4.97 min, *m/z* = 280.21 $[M+H]^+$ (*E*)-isomer. λ_{max} = 285, 425 nm [(*Z*)-isomer]; 319 nm [(*E*)-isomer)]. HRMS [ESI^+] m/z = 279.17353 $[M]^+$, calcd for $[C_{18}H_{21}N_3]^+$ 279.17355.

*4.4. General procedure for the synthesis of azocuronium salts m-**1**(**a**-**e**), p-**1**(**a**,**b**) and m-**5b***

A solution of the appropriate diazene compound *m*-**3**(**a**-**d**), *p*-**3**(**a**,**b**) or *m*-**4b** (1 equiv.) and CH_3I (1.25 equiv. per amine) in anhydrous DMF (1.5 mL/mmol) was heated under mw irradiation at 120 ºC for 12 min. Solvent was evaporated under reduced pressure and the residue was solved in H_2O and washed with EtOAc. The aqueous layer was lyophilized to give the desired azocuronium salt that was crystallized in methanol.

*4.4.1. 1,1'-{[Diazene-1,2-diylbis(3,1-phenylene)]bis(methylene)}bis(1-methylpyrrolidin-1-ium) diiodide (m-**1a**)*

Following the general procedure, from diazene *m*-**3a** (50 mg, 0.14 mmol) and CH_3I (26 μL, 0.40 mmol) azocuronium salt *m*-**1a** was obtained as an orange solid (47 mg, 89% yield) of mp 53-55 ºC. (*E*)-Isomeric purity: 98%. ^{1}H NMR (500 MHz, CD_3OD): δ 8.24 (d, *J* = 1.6 Hz, 2H, H_o), 8.13 (dd, *J* = 7.9, 1.6 Hz, 2H, $H_{o'}$), 7.81 (dd, *J* = 7.6, 1.5 Hz, 2H, H_p), 7.75 (t, *J* = 7.7 Hz, 2H, $H_{m'}$), 4.77 (s, 4H, H_α), 3.79 (dt, *J* = 12.5, 7.0 Hz, 4H, H_{2eq}), 3.60 – 3.52 (m, 4H, H_{2ax}), 3.09 (s, 6H, H_β), 2.39 – 2.24 (m, 8H, H_3). ^{13}C NMR (126 MHz, CD_3OD): δ 154.2 (C_i), 136.5 (C_p), 131.5 ($C_{m'}$), 131.3 (C_m), 128.2 (C_o), 125.8 ($C_{o'}$), 67.4 (C_α), 65.0 (C_2), 48.8 (C_β), 22.3 (C_3). λ_{max} = 319 nm [(*E*)-isomer]. HRMS [ESI+] m/z = 378.27908 $[M]^{2+}$, calcd for $[C_{24}H_{34}N_4]^{2+}$ m/z = 378.27835.

*4.4.2. 1,1'-{[Diazene-1,2-diylbis(4,1-phenylene)]bis(methylene)}bis(1-methylpyrrolidin-1-ium) diiodide (p-**1a**)*

According to the general method, from diazene *p*-**3a** (50 mg, 0.14 mmol) and CH_3I (26 μL, 0.40 mmol) azocuronium salt *p*-**1a** was obtained as an orange solid (46 mg, 88% yield) of mp 153-156 ºC. (*E*)-Isomeric purity: 99%. ^{1}H NMR (400 MHz, CD_3OD): δ 8.08 (d, *J* = 8.4 Hz, 4H, H_o), 7.85 (d, *J* = 8.4 Hz, 4H, H_m), 4.74 (s, 4H, H_α), 3.81 – 3.70 (m, 4H, H_{2eq}), 3.60 – 3.51 (m, 4H, H_{2ax}), 3.07 (s, 6H, H_β), 2.38 – 2.24 (m, 8H, H_3). ^{13}C NMR (101 MHz, CD_3OD): δ 154.8 (C_i), 134.9 (C_m), 133.1 (C_p), 124.6 (C_o), 67.1 (C_α), 64.9 (C_2), 48.6 (C_β), 22.3 (C_3). λ_{max} = 322 nm [(*E*)-isomer]. HRMS [ESI+] m/z = 378.27836 $[M]^{2+}$, calcd for $[C_{24}H_{34}N_4]^{2+}$ m/z = 378.27835.

*4.4.3. 1,1'-{[Diazene-1,2-diylbis(3,1-phenylene)]bis(methylene)}bis(1-methylpiperidin-1-ium) diiodide (m-**1b**)*

Following the general procedure, from diazene *m*-**3b** (45 mg, 0.12 mmol) and CH_3I (17.9 μL, 0.49 mmol) azocuronium salt *m*-**1b** was obtained as an orange solid (67 mg, 85% yield) of mp 174-176 ºC. (*E*)-Isomer purity: 95%. ^{1}H NMR (500 MHz, CD_3OD) (*E*)-isomer: δ 8.24 (bs, 2H, H_o), 8.14 (dt, *J* = 7.6, 1.7 Hz, 2H, $H_{o'}$), 7.79 (dt, *J* = 7.7, 1.6 Hz, 2H, H_p), 7.75 (t, *J* = 7.6 Hz, 2H, $H_{m'}$), 4.78 (s, 4H, H_α), 3.55 (m, 4H, H_{2eq}), 3.50 – 3.42 (m, 4H, H_{2ax}), 3.10 (s, 6H, H_β), 2.08 – 1.93 (m, 8H, H_3), 1.87 – 1.76 (m, 2H, H_{4eq}), 1.76 – 1.61 (m, 2H, H_{4ax}). ^{13}C NMR (126 MHz, CD_3OD) (*E*)-isomer: δ 154.0 (C_i), 137.1 (C_p), 131.4 ($C_{m'}$), 130.0 (C_m), 129.0 (C_o), 125.8 ($C_{o'}$), 68.6 (C_α), 62.1 (C_2), 47.2 (C_β), 22.2 (C_4), 21.1 (C_3). After UV irradiation, (*Z*)-isomer was obtained with a purity of 96%. ^{1}H NMR (500 MHz, CD_3OD) (*Z*)-isomer: δ 7.57 (d, *J* = 7.8 Hz, 2H, $H_{m'}$), 7.45 – 7.43 (d, *J* = 7.8 Hz, 2H, H_p), 7.36 (d, *J* = 8.1 Hz, 2H, $H_{o'}$), 6.93 (s, 2H, H_o), 4.39 (s, 4H, H_α), 3.14 (t, *J* = 5.8 Hz, 8H, H_2), 2.78 (s, 6H, H_β), 1.89 – 1.82 (m, 8H, H_3), 1.77 – 1.69 (m, 2H, H_{4eq}), 1.57 – 1.46 (m, 2H, H_{4ax}). ^{13}C NMR (126 MHz, CD_3OD) (*Z*)-isomer: δ 152.5 (C_i), 132.6 (C_p), 130.1 ($C_{m'}$), 127.8 (C_m), 123.8 (C_o), 123.7 ($C_{o'}$), 67.0 (C_α), 60.6 (C_2), 46.1 (C_β), 30.1, 20.4 (C_4), 19.4 (C_3). λ_{max} = 320 nm [(*E*)-isomer]. HRMS [ESI^+] m/z = 406.31014 $[M]^{2+}$, calcd for $[C_{26}H_{38}N_4]^{2+}$ m/z = 406.30965.

*4.4.4. 1,1'-{[Diazene-1,2-diylbis(4,1-phenylene)]bis(methylene)}bis(1-methylpiperidin-1-ium) diiodide (p-**1b**)*

Following the general procedure, from diazene *p*-**3b** (31 mg, 0.08 mmol) and CH_3I (14.35 μL, 0.23 mmol) azocuronium salt *p*-**1b** was obtained as an orange solid (43 mg, 82% yield) of mp 291-231 ºC. (*E*)-Isomer purity: 95%. ^{1}H NMR (300 MHz, CD_3OD): δ 8.09 (d, *J* = 8.4 Hz, 4H, H_o), 7.82 (d, *J* = 8.4 Hz, 4H, H_m), 4.72 (s, 4H, H_α), 3.58 – 3.47 (m, 4H, $H_{2\ eq}$), 3.46 – 3.36 (m, 4H, H_{2ax}), 3.08 (s, 6H, H_β), 2.08 – 1.94 (m, 8H, H_3), 1.87 – 1.75 (m, 2H, $H_{4\ eq}$), 1.75 – 1.64 (m, 2H, $H_{4\ ax}$). ^{13}C NMR (75 MHz, CD_3OD): δ 54.8 (C_i), 135.5 (C_o), 131.8 (C_p), 124.5 (C_m), 68.4 (C_α), 62.2 (C_2), 55.9 (C_β), 22.2 (C_4), 21.1 (C_3). λ_{max} = 321 nm [(*E*)-isomer]. HRMS [ESI^+] m/z = 406.30984 $[M]^{2+}$, calcd for $[C_{26}H_{38}N_4]^{2+}$ 406.30965.

*4.4.5. 1,1'-{[Diazene-1,2-diylbis(3,1-phenylene)]bis(methylene)}bis(1-methylazepan-1-ium) diiodide (m-**1c**)*

Following the general method, from diazene *m*-**3c** (80 mg, 0.20 mmol) and CH_3I (18.3 μL, 0.50 mmol) azocuronium salt *m*-**1c** was obtained as a yellow-orange solid (115 mg, 90%) of mp 145 ºC (decomposes). (*E*)-Isomeric purity: 98%. ^{1}H NMR (500 MHz, D_2O) (*E*)-isomer: δ 8.09 – 8.06 (m, 2H, $H_{o'}$), 8.06 (bs, 2H, H_o), 7.76 – 7.73 (m, 4H, $H_{m'}$, H_p), 4.63 (s, 4H, H_α), 3.62 (dt, *J* = 14.2, 5.0 Hz, 4H, H_{2eq}, H_{7eq}), 3.39 (dt, *J* = 14.0, 4.8 Hz, 4H, H_{2ax}, H_{7ax}), 3.03 (s, 6H, CH_3), 1.99 – 1.90 (m, 8H, H_3, H_6), 1.75 – 1.68 (m, 8H, H_4, H_5). ^{13}C NMR (126 MHz, D_2O) (*E*)-isomer: δ 152.9 (C_i), 136.7 (C_p), 131.0 ($C_{m'}$), 129.5 (C_m), 127.6 (C_o), 125.1 ($C_{o'}$), 68.5 (C_α), 64.7 (C_2, C_7), 50.6 (CH_3), 28.0 (C_4, C_5), 21.8 (C_3, C_6). (*Z*) δ 153.3 (C_i), 133.3 (C_p), 130.8 ($C_{m'}$), 129.5 (C_m), 124.7 (C_o), 124.2 ($C_{o'}$), 64.6 (C_2, C_7), 50.3

(CH_3), 27.9 (C_4, C_5), 21.7 (C_3, C_6). (*Z*)-Isomer was obtained after UV irradiation. ^{1}H NMR (500 MHz, D_2O) (*Z*)-isomer: δ 7.55 (t, *J* = 7.9 Hz, 2H, $H_{m'}$), 7.43 (d, *J* = 7.7 Hz, 2H, H_p), 7.30 (d, *J* = 8.0, 1.9 Hz, 2H, $H_{o'}$), 6.97 (s, 2H, H_o), 4.36 (s, 4H, H_α), 3.30 (dt, *J* = 14.0, 5.0 Hz, 4H, H_{2eq}, H_{7eq}), 3.16 (dt, *J* = 14.0, 4.8 Hz, 4H, H_{2ax}, H_{7ax}), 2.76 (s, 6H, CH_3), 1.85 – 1.78 (m, 8H, H_3, H_6), 1.67 – 1.61 (m, 8H, H_4, H_5). ^{13}C NMR (126 MHz, D_2O) (*Z*)-isomer: δ 153.3 (C_i), 133.3 (C_p), 130.8 ($C_{m'}$), 129.5 (C_m), 124.7 (C_o), 124.2 ($C_{o'}$), 64.6 (C_2, C_7), 50.3 (CH_3), 27.9 (C_4, C_5), 21.7 (C_3, C_6). λ_{max} = 319 nm [(*E*)-isomer]. HRMS [ESI^+] m/z = 434.34076 $[M]^{2+}$, calcd for $[C_{28}H_{42}N_4]^{2+}$ 434.34095.

*4.4.6. 1,1'-{[Diazene-1,2-diylbis(3,1-phenylene)]bis(methylene)}bis(1-methyl-1,2,3,6-tetrahydropyridin-1-ium) diiodide (m-**1d**)*

Following the general procedure, from diazene *m*-**3d** (60 mg, 0.16 mmol) and and CH_3I (14.6 μL, 0.40 mmol) azocuronium salt *m*-**1d** was obtained as a yellow-orange solid (82 mg, 78% yield) of mp: 200 ºC (decomposes). (*E*)-Isomeric purity >99%. ^{1}H NMR (500 MHz, D_2O) (*E*)-isomer: δ 8.12 – 8.09 (m, 2H, H_o), 8.08 (bs, 2H, $H_{o'}$), 7.79 – 7.76 (m, 4H, H_p, $H_{m'}$), 6.10 (d, *J* = 10.2 Hz, 2H, H_4), 5.78 (d, *J* = 10.0 Hz, 2H, H_3), 4.75 (d, *J* = 13.2 Hz, 4H, 1H_α), 4.63 (d, *J* = 13.2 Hz, 2H, 1H_α), 4.10 (d, *J* = 16.5 Hz, 2H, H_{2eq}), 3.78 (d, *J* = 16.4 Hz, 2H, H_{2ax}), 3.67 – 3.56 (m, 4H, H_6), 3.09 (s, 6H, H_β), 2.65 – 2.56 (m, 4H, H_5). ^{13}C NMR (126 MHz, D_2O) (*E*)-isomer: δ 153.0 (C_i), 136.7 (C_p), 131.0 ($C_{m'}$), 128.8 (C_m), 127.6 (C_o), 125.6 (C_4), 125.3 ($C_{o'}$), 118.9 (C_3), 67.5 (C_α), 58.7 (C_2), 57.8 (C_6), 47.4 (C_β), 21.6 (C_5). After UV irradiation, (*Z*)-isomer was obtained. ^{1}H NMR (500 MHz, D_2O) (*Z*)-isomer: δ 7.60 (t, *J* = 7.9 Hz, 2H, $H_{m'}$), 7.46 (d, *J* = 7.8 Hz, 2H, H_p), 7.39 (d, *J* = 8.2 Hz, 2H, $H_{o'}$), 6.94

(s, 2H, H_o), 6.03 (d, *J* = 10.4 Hz, 2H, H_4), 5.66 (d, *J* = 10.6 Hz, 2H, H_3), 4.47 (d, *J* = 13.2 Hz, 2H, 1H_α), 4.37 (d, *J* = 13.1 Hz, 2H, 1H_α), 3.71 (d, *J* = 16.5 Hz, 2H, H_{2eq}), 3.53 (d, *J* = 16.5 Hz, 2H, H_{2ax}), 3.39 – 3.32 (m, 2H, H_6), 3.22 (dt, *J* = 12.9, 6.2 Hz, 2H, H_6), 2.83 (s, 6H, H_β), 2.48 (s, 4H, H_5). ^{13}C NMR (126 MHz, D_2O) (*Z*)-isomer: δ 153.3 (C_i), 133.3 (C_p), 130.9 ($C_{m'}$), 128.3 (C_m), 125.5 (C_4), 124.6 ($C_{o'}$), 124.5 (C_o), 118.6 (C_3), 67.2 (C_α), 58.4 (C_2), 57.4 (C_6), 47.2 (C_β), 21.5 (C_5). λ_{max} = 321 nm [(*E*)-isomer]. HRMS [ESI$^+$] m/z = 402.27886 $[M]^{2+}$, calcd for $[C_{26}H_{34}N_4]^{2+}$ 402.27835.

*4.4.7. 1-Methyl-1-[3-(phenyldiazenyl)benzyl]piperidin-1-ium iodide (m-**5b**)*

Following the general procedure, from diazene *m*-**4b** (125 mg, 0.45 mmol) and and CH_3I (41.2 μL, 1.13 mmol) azocuronium salt *m*-**1d** was obtained as brown oil (110 mg, 58% yield). (*E*)-Isomer purity >99%. ^{1}H NMR (500 MHz, CD_3OD): δ 8.09 (t, *J* = 1.8 Hz, 1H, H_o), 8.07 (d, *J* = 7.8 Hz, 1H, $H_{o'}$), 7.97 – 7.93 (m, 2H, $H_{o''}$), 7.71 (t, *J* = 7.6 Hz, 1H, $H_{m'}$), 7.70 – 7.64 (m, 1H, H_p), 7.59 – 7.54 (m, 3H, $H_{m''}$, $H_{p'}$), 4.44 (s, 2H, H_α), 3.54 – 3.49 (m, 2H, H_{2eq}), 3.03 (dd, *J* = 12.0, 2.6 Hz, 2H, H_{2eq}), 2.70 (s, 3H, CH_3), 1.97 (dt, *J* = 15.4, 2.6 Hz, 2H, H_{3eq}), 1.85 (dt, *J* = 13.1, 3.8 Hz, 1H, H_{4eq}), 1.79 – 1.73 (m, 2H, H_{3ax}), 1.54 (dt, *J* = 12.7, 3.8 Hz, 1H, H_{4ax}). ^{13}C NMR (126 MHz, CD_3OD): δ 154.4 (C_i), 153.8 ($C_{i'}$), 134.8 (C_p), 132.9 ($C_{p'}$), 131.7 (C_m), 131.4 ($C_{m'}$), 130.4 ($C_{m''}$), 126.0 (C_o), 125.8 ($C_{o'}$), 123.9 ($C_{o''}$), 61.4 (C_α), 54.2 (C_2), 35.4 (CH_3), 24.1 (C_3). λ_{max} = 318 nm [(*E*)-isomer]. HRMS [ESI$^+$] m/z = 294.19714 $[M]^+$, calcd for $[C_{19}H_{24}N_3]^+$ 294.19702.

4.5. Thermodynamic solubility studies

The solubility experiments were performed following described protocols [32,33]. From UV-spectra of compounds maximums were determined between wavelengths 270 and 400 nm. A 10 mM stock solution of the corresponding compound in pH 7.4 phosphate 45 mM buffer was prepared and a calibration line was built by measuring the absorbance at the corresponding maximum wavelength of sequential dilutions of the stock solution in buffer in a 96-well plate containing 200 µL per point. The calibration line was accepted if R^2>0.990, the residual value of each point <15% and the relative error of the quality control standard <15%. The solubility determination was made as follows: 200 µL of buffer solution were added over approximately 1 mg accurately weighted of the corresponding compound in order to achieve a saturated solution. The mixture was kept at rt in an orbital stirrer at 320 rpm for 24h and then centrifuged at 135 rpm for 15 min. 160 µL of the supernatant were transferred to a 96-well plate and diluted with 40 µL of buffer. The solubility was determined by extrapolation to the calibration line within the linearity range and expressed in mol/L. The experiments were run in triplicates.

4.6. In vitro evaluation of the CNS-penetration (PAMPA-BBB assay)

Prediction of the brain penetration was evaluated using the PAMPA-BBB assay, in a similar manner as previously described [34-40]. Pipetting was performed with a semi-automatic robot (CyBi®-SELMA) and UV reading with a microplate spectrophotometer (Multiskan Spectrum, Thermo Electron Co.). Commercial drugs, phosphate buffered saline solution at pH 7.4 (PBS), and dodecane were purchased from Sigma, Aldrich, Acros, and

Fluka. Millex filter units (PVDF membrane, diameter 25 mm, pore size 0.45 μm) were acquired from Millipore. The porcine brain lipid (PBL) was obtained from Avanti Polar Lipids. The donor microplate was a 96-well filter plate (PVDF membrane, pore size 0.45 μm) and the acceptor microplate was an indented 96-well plate, both from Millipore. The acceptor 96-well microplate was filled with 200 μL of PBS: EtOH (70:30) and the filter surface of the donor microplate was impregnated with 4 μL of porcine brain lipid (PBL) in dodecane (20 mg mL^{-1}). Compounds were dissolved in PBS: EtOH (70:30) at 100 μg mL^{-1}, filtered through a Millex filter, and then added to the donor wells (200 μL). The donor filter plate was carefully put on the acceptor plate to form a sandwich, which was left undisturbed for 240 min at 25 ºC. After incubation, the donor plate is carefully removed and the concentration of compounds in the acceptor wells was determined by UV/vis spectroscopy. Every sample is analyzed at five wavelengths, in four wells and at least in three independent runs, and the results are given as the mean ± standard deviation. In each experiment, 11 quality control standards of known BBB permeability were included to validate the analysis set.

4.7. Measurement of cell viability with MTT

Cell viability, virtually the mitochondrial activity of living cells, was measured by quantitative colorimetric assay with MTT (3-[4,5- dimethylthiazol-2-yl]-2,5-diphenyltetrazolium bromide, Sigma Aldrich, Madrid, Spain), based on the ability of viable cells to reduce yellow MTT to blue formazan as described previously [41]. Briefly, cells were plated in wells of 96-well plates and incubated in presence of compounds at 37 °C for

24 h. At the end of the treatment, the medium was removed and the cells were incubated with 100 µl of MTT (5 mg/ml in phosphate buffered saline; PBS) in a fresh medium for 4 h at 37 °C. After 4 h, formazan crystals, formed by mitochondrial reduction of MTT, were solubilized in DMSO (150 µL per well). After mixing, the absorbance of the cells was measured at 540 nm.

4.8. Photochemical characterization by UV/vis

A solution of the corresponding azocuronium salt in H_2O (100 µM) was placed in a 1 mL quartz cuvette (10 mm diameter) and absorption spectrum was recorded in a diodo-array UV-vis spectrophotometer (DH2000) under thermal relaxed conditions. Then, the solution was irradiated under either UV or blue light with a LED and the UV-vis spectrum was registered again.

4.9. Radioligand binding assays at muscle-type nAChRs expressed in TE671 cells

Cell membrane homogenates (60 µg protein) are incubated for 120 min at 22 °C with 0.5 nM [^{125}I]α-bungarotoxin in the absence or presence of the tested compound in a buffer solution containing 20 mM Hepes/NaOH (pH 7.3), 118 mM NaCl, 4.8 mM KCl, 2.5 mM $CaCl_2$, 1.2 mM $MgSO_4$ and 0.1% BSA. Nonspecific binding is determined in the presence of 5 µM α-bungarotoxin. Following incubation, the samples are filtered rapidly under vacuum through glass fiber filters (GF/B, Packard) presoaked with 0.3% PEI and rinsed several times with an ice-cold buffer containing 50 mM Tris-HCl, 500 mM NaCl and 0.1%

BSA using a 96-sample cell harvester (Unifilter, Packard). The filters are dried then counted for radioactivity in a scintillation counter (Topcount, Packard) using a scintillation cocktail (Microscint 0, Packard). The results are expressed as a percent inhibition of the control radioligand specific binding. The standard reference compound is α-bungarotoxin, which is tested in each experiment at several concentrations to obtain a competition curve from which its IC_{50} is calculated [49].

4.10. Radioligand binding assays at α7 neuronal nAChRs expressed in transfected SH-SY5Y cells

Cell membrane homogenates (20 µg protein) are incubated for 120 min at 37 °C with 0.05 nM [^{125}I]-bungarotoxin in the absence or presence of the tested compound in a buffer solution containing 50 mM K_2HPO_4/KH_2PO_4 (pH 7.4), 10 mM $MgCl_2$ and 0.1% BSA. Nonspecific binding is determined in the presence of 1 µM α-bungarotoxin. After incubation, the samples are filtered rapidly under vacuum through glass fiber filters (GF/B, Packard) presoaked with 0.3% PEI and rinsed several times with ice-cold 50 mM Tris-HCl and 150 mM NaCl using a 96-sample cell harvester (Unifilter, Packard). The filters are dried then counted for radioactivity in a scintillation counter (Topcount, Packard) using a scintillation cocktail (Microscint 0, Packard). The results are expressed as a percent inhibition of the control radioligand specific binding. The standard reference compound is (+/-)-epibatidine, which is tested in each experiment at several concentrations to obtain a competition curve from which its IC_{50} is calculated [50].

4.11. Radioligand binding assays at α4β2 neuronal nAChRs expressed in transfected SH-SY5Y cells

Cell membrane homogenates (60 µg protein) are incubated for 120 min at 22 °C with 0.5 nM [^{125}I]α-bungarotoxin in the absence or presence of the tested compound in a buffer solution containing 20 mM Hepes/NaOH (pH 7.3), 118 mM NaCl, 4.8 mM KCl, 2.5 mM $CaCl_2$, 1.2 mM $MgSO_4$ and 0.1% BSA. Nonspecific binding is determined in the presence of 5 µM α-bungarotoxin. Following incubation, the samples are filtered rapidly under vacuum through glass fiber filters (GF/B, Packard) presoaked with 0.3% PEI and rinsed several times with an ice-cold buffer containing 50 mM Tris-HCl, 500 mM NaCl and 0.1% BSA using a 96-sample cell harvester (Unifilter, Packard). The filters are dried then counted for radioactivity in a scintillation counter (Topcount, Packard) using a scintillation cocktail (Microscint 0, Packard). The results are expressed as a percent inhibition of the control radioligand specific binding. The standard reference compound is α-bungarotoxin, which is tested in each experiment at several concentrations to obtain a competition curve from which its IC_{50} is calculated [51].

4.12. Preparation of oocytes and RNA injections

Xenopus laevis oocyte isolation, preparation and RNA injection were performed using methods published from the lab and elsewhere [52,53]. Animal protocols were approved by Institutional Animal Care and Use Committees at University of the Pacific and conform to the requirements in the Guide for the Care and Use of Laboratory Animals from the U.S. National Academy of Sciences. Frogs were purchased from *Xenopus* 1 (Dexter, MI).

Oocytes were maintained at 16-17 ^{o}C in an incubation solution of (in mM): 99 NaCl, 1 KCl, 2 $CaCl_2$, 1 $MgCl_2$ or $MgSO_3$, 10 HEPES, 2 pyruvic acid, and 20-50 mg/L of gentamycin. The incubation solution was titrated to pH 7.5 with NaOH. Results from many batches of oocytes were combined.

For expression, plasmids encoding for the α_1, β_1, δ_1, and γ_1 subunits of the embryonic nAChR from rat were prepared in the laboratory from original samples kindly gifted by Dr. Roger Papke. The plasmids were transcribed into cRNA using a SP6 RNA polymerase kit (mMessage mMachine, Ambion). Oocytes were injected with a mix containing 2.5 ng of each *in vitro*-transcribed cRNA. Injected oocytes were kept in incubation solution at 16-17 ^{o}C for 2-4 days before recordings.

4.13. Electrophysiology

Ionic currents were recorded using the two-electrode voltage-clamp (TEVC) technique employing a GeneClamp amplifier (Axon Instruments). For these recordings, the membrane potential was held at -60 mV with constant perfusion by recirculation. Two custom-made LEDs system built in the Villalba-Galea lab were used to drive photoisomerization. The LEDs were powered with 3.5-5V linear power sources. Their emission spectra were centered at 335-340 nm (UV light, Marktech Optoelectronics, MTE340H21-UV) and 400-450 nm (blue light, Marktech Optoelectronics, MT0380-UV-A, MTE4600P) were used to induce photo-isomerization of the compounds. All LED emission spectra had a 20-35 nm full width at half maximum per manufacturer specifications. The

LEDs were powered using an in house-built circuit controlled by the acquisition system to synchronize LED irradiation with the electrophysiological recordings.

Receptor activation was driven by external application of ACh using a nano-injector (Nanoject II, Drummond Scientific) with a sharpen glass capillary. Briefly, 2.3 to 18.4 nL of 50 μM of ACh were applied on the surface of the oocytes at a rate of 46 nL/s. These "puffs" of ACh were allowed to freely diffuse for 100-1000 ms and subsequently washed out by recording solution recirculation. The wide range of "puff" volume used were adjusted to maximize response from the oocytes as 50 μM of ACh was already a saturating concentration for these receptors, as embryonic nAChR display an affinity for ACh below 10 μM [9]. An in house-made micro-recirculation system was built using a piezoelectric-based peristaltic pump (Bartels Mikrotechnik, Germany). The powering system for the pump was controlled by the acquisition system. The chamber volume was 100-150 μL and the total "dead" volume of the tubing and pump was 100 μL.

For TEVC recordings, oocytes were bathed in a recording solution containing (in mM): 99 NaCl, 1 KCl, 2 $CaCl_2$, 1 $MgCl_2$ or $MgSO_3$, and 10 HEPES titrated to pH 7.4 with NaOH. Glass sharp electrodes (resistance = 0.2-2.0 MΩ) were filled with a solution containing (in mM) 1000 KCl, 10 HEPES and 10 EGTA, at pH 7.4 (KOH). Voltage control and current acquisition was performed using a USB-6251 multi-function acquisition board (National Instruments) controlled by an in house-made program coded in LabVIEW (National Instruments) (C.A. Villalba-Galea, details available upon request). In addition, the nano-injector delivering the "ACh puffs", the LEDs and the micro-recirculation system were controlled with the multi-function board to synchronize their actions. Current signals were filtered at 100 kHz, oversampled at 1-2 MHz, and stored at 5-25 kHz for offline analysis.

Data were analyzed using a custom Java-based software (C.A. Villalba-Galea, details available upon request) and Origin 2018 (OriginLab).

5. Acknowledgments

The authors gratefully acknowledge the following financial supports: Spanish Ministry of Science, Innovation and Universities; Spanish Research Agency; and European Regional Development Funds (grants SAF2015-64948-C2-1-R and RTI2018-093955-B-C21 to MIRF), General Council for Research and Innovation of the Community of Madrid and European Structural Funds (grant S2017/BMD-3827 – NRF24ADCM to MIRF) and Spanish National Research Council CSIC (grant PIE-202080E118). CH-A also thanks her PhD fellowships from Spanish Ministry of Education (MEC, PhD grant FPU16/01704 and mobility grant FPUEST17/00233).

6. References

[1] D. Paterson, A. Nordberg, Neuronal nicotinic receptors in the human brain, Prog. Neurobiol. 61 (2000) 75-111.

[2] B.E. Nielsen, I. Bermudez, C. Bouzat, Flavonoids as positive allosteric modulators of alpha7 nicotinic receptors, Neuropharmacology 160 (2019) 107794.

[3] A. Karlin, E. Holtzman, N. Yodh, P. Lobel, J. Wall, J. Hainfeld, The arrangement of the subunits of the acetylcholine receptor of *Torpedo californica*, J. Biol. Chem. 258 (1983) 6678-6681.

[4] N. Unwin, Nicotinic acetylcholine receptor and the structural basis of neuromuscular transmission: insights from Torpedo postsynaptic membranes, Q. Rev. Biophys. 46 (2013) 283-322.

[5] M. Mishina, T. Takai, K. Imoto, M. Noda, T. Takahashi, S. Numa, C. Methfessel, B. Sakmann, Molecular distinction between fetal and adult forms of muscle acetylcholine receptor, Nature 321 (1986) 406.

[6] V. Witzemann, B. Barg, Y. Nishikawa, B. Sakmann, S. Numa, Differential regulation of muscle acetylcholine receptor γ-and ϵ-subunit mRNAs, FEBS Lett. 223 (1987) 104-112.

[7] J.M. Hunter, Reversal of residual neuromuscular block: complications associated with perioperative management of muscle relaxation, Br. J. Anaesth. 119 (2017) i53-i62.

[8] M.M. Lerch, M.J. Hansen, G.M. van Dam, W. Szymanski, B.L. Feringa, Emerging targets in Photopharmacology, Angew. Chem. Int. Ed. Engl. 55 (2016) 10978-10999.

[9] T.K. Nayak, I. Bruhova, S. Chakraborty, S. Gupta, W. Zheng, A. Auerbach, Functional differences between neurotransmitter binding sites of muscle acetylcholine receptors, Proc. Natl. Acad. Sci. USA 111 (2014) 17660-17665.

[10] M. Cecchini, J.P. Changeux, The nicotinic acetylcholine receptor and its prokaryotic homologues: Structure, conformational transitions & allosteric modulation, Neuropharmacology 96 (2015) 137-149.

[11] W.C. Bowman, Neuromuscular block, Br. J. Pharmacol. 147 Suppl 1 (2006) S277-286.

[12] K. Farooq, J.M. Hunter, Neuromuscular blocking agents and reversal agents, Anaesth. Intens. Care Med. 18 (2017) 279-284.

[13] E. Bartels, N.H. Wassermann, B.F. Erlanger, Photochromic activators of the acetylcholine receptor, Proc. Natl. Acad. Sci. USA 68 (1971) 1820-1823.

[14] J.M. Nerbonne, R.E. Sheridan, L. Chabala, H.A. Lester, cis-3, 3'-Bis-[alpha-(trimethylammonium) methyl] azobenzene (cis-Bis-Q). Purification and properties at acetylcholine receptors of *Electrophorus* electroplaques, Mol. Pharmacol. 23 (1983) 344-349.

[15] X. Gomez-Santacana, J.A.R. Dalton, X. Rovira, J.P. Pin, C. Goudet, P. Gorostiza, J. Giraldo, A. Llebaria, Positional isomers of bispyridine benzene derivatives induce efficacy changes on mGlu5 negative allosteric modulation, Eur. J. Med. Chem. 127 (2017) 567-576.

[16] S.K. Rastogi, Z. Zhao, S.L. Barrett, S.D. Shelton, M. Zafferani, H.E. Anderson, M.O. Blumenthal, L.R. Jones, L. Wang, X. Li, C.N. Streu, L. Du, W.J. Brittain, Photoresponsive azo-combretastatin A-4 analogues, Eur. J. Med. Chem. 143 (2018) 1-7.

[17] T. Lutz, T. Wein, G. Höfner, J. Pabel, M. Eder, J. Dine, K.T. Wanner, Development of new photoswitchable azobenzene based γ-aminobutyric acid (GABA) uptake inhibitors with distinctly enhanced potency upon photoactivation, J. Med. Chem. 61 (2018) 6211-6235.

[18] P. Leippe, N. Winter, M.P. Sumser, D. Trauner, Optical control of a delayed rectifier and a two-pore potassium channel with a photoswitchable bupivacaine, ACS Chem. Neurosci. 9 (2018) 2886-2891.

[19] R. Ferreira, J.R. Nilsson, C. Solano, J. Andréasson, M. Grøtli, Design, synthesis and inhibitory activity of photoswitchable RET kinase inhibitors, Sci. Rep. 5 (2015) 9769.

[20] M.W.H. Hoorens, M.E. Ourailidou, T. Rodat, P.E. van der Wouden, P. Kobauri, M. Kriegs, C. Peifer, B.L. Feringa, F.J. Dekker, W. Szymanski, Light-controlled inhibition of BRAFV600E kinase, Eur. J. Med. Chem. 179 (2019) 133-146.

[21] S. Pittolo, H. Lee, A. Lladó, S. Tosi, M. Bosch, L. Bardia, X. Gómez-Santacana, A. Llebaria, E. Soriano, J. Colombelli, K.E. Poskanzer, G. Perea, P. Gorostiza, Reversible silencing of endogenous receptors in intact brain tissue using 2-photon pharmacology, Proc. Natl. Acad. Sci. USA 116 (2019) 13680.

[22] M. Ricart-Ortega, J. Font, A. Llebaria, GPCR photopharmacology, Mol. Cell. Endocrinol. 488 (2019) 36-51.

[23] L. Laprell, I. Tochitsky, K. Kaur, M.B. Manookin, M. Stein, D.M. Barber, C. Schon, S. Michalakis, M. Biel, R.H. Kramer, M.P. Sumser, D. Trauner, R.N. Van Gelder, Photopharmacological control of bipolar cells restores visual function in blind mice, J. Clin. Invest. 127 (2017) 2598-2611.

[24] I. Tochitsky, M.A. Kienzler, E. Isacoff, R.H. Kramer, Restoring vision to the blind with chemical photoswitches, Chem. Rev. 118 (2018) 10748-10773.

[25] G. Chemi, M. Brindisi, S. Brogi, N. Relitti, S. Butini, S. Gemma, G. Campiani, A light in the dark: state of the art and perspectives in optogenetics and optopharmacology for restoring vision, Future Med. Chem. 11 (2019) 463-487.

[26] I. Tochitsky, Z. Helft, V. Meseguer, R.B. Fletcher, K.A. Vessey, M. Telias, B. Denlinger, J. Malis, E.L. Fletcher, R.H. Kramer, How azobenzene photoswitches restore visual responses to the blind retina, Neuron 92 (2016) 100-113.

[27] P. Bregestovski, G. Maleeva, P. Gorostiza, Light-induced regulation of ligand-gated channel activity, Br. J. Pharmacol. 175 (2018) 1892-1902.

[28] L. Sansalone, J. Zhao, M.T. Richers, G.C.R. Ellis-Davies, Chemical tuning of photoswitchable azobenzenes: a photopharmacological case study using nicotinic transmission, Beilstein J. Org. Chem. 15 (2019) 2812-2821.

[29] D. Lemoine, R. Durand-de Cuttoli, A. Mourot, Optogenetic control of mammalian ion channels with chemical photoswitches, Methods Mol. Biol. 1408 (2016) 177-193.

[30] A. Damijonaitis, J. Broichhagen, T. Urushima, K. Hüll, J. Nagpal, L. Laprell, M. Schönberger, D.H. Woodmansee, A. Rafiq, M.P. Sumser, W. Kummer, A. Gottschalk, D. Trauner, AzoCholine enables optical control of alpha 7 nicotinic acetylcholine receptors in neural networks, ACS Chem. Neurosci. 6 (2015) 701-707.

[31] T. Severin, R. Schmitz, M. Adam, Umsetzung von nitroaromaten mit natriumborhydrid, IV, Chem. Ber. 96 (1963) 3076-3080.

[32] H. Tan, D. Semin, M. Wacker, J. Cheetham, An automated screening assay for determination of aqueous equilibrium solubility enabling SPR study during drug lead optimization, J. Assoc. Lab. Autom. 10 (2005) 364-373.

[33] B. Bard, S. Martel, P.-A. Carrupt, High throughput UV method for the estimation of thermodynamic solubility and the determination of the solubility in biorelevant media, Eur. J. Pharm. Sc. 33 (2008) 230-240.

[34] L. Di, E.H. Kerns, K. Fan, O.J. McConnell, G.T. Carter, High throughput artificial membrane permeability assay for blood-brain barrier, Eur. J. Med. Chem. 38 (2003) 223-232.

[35] M.I. Fernández-Bachiller, C. Pérez, L. Monjas, J. Rademann, M.I. Rodríguez-Franco, New tacrine--4-oxo-4*H*-chromene hybrids as multifunctional agents for the treatment of Alzheimer's disease, with cholinergic, antioxidant, and beta-amyloid-reducing properties, J. Med. Chem. 55 (2012) 1303-1317.

[36] B. López-Iglesias, C. Pérez, J.A. Morales-García, S. Alonso-Gil, A. Pérez-Castillo, A. Romero, M.G. López, M. Villarroya, S. Conde, M.I. Rodríguez-Franco, New melatonin--*N*,*N*-dibenzyl(*N*-methyl)amine hybrids: potent neurogenic agents with antioxidant, cholinergic, and neuroprotective properties as innovative drugs for Alzheimer's disease, J. Med. Chem. 57 (2014) 3773-3785.

[37] M. Estrada, C. Herrera-Arozamena, C. Pérez, D. Viña, A. Romero, J.A. Morales-García, A. Pérez-Castillo, M.I. Rodríguez-Franco, New cinnamic - *N*-benzylpiperidine and cinnamic - *N*,*N*-dibenzyl(*N*-methyl)amine hybrids as Alzheimer-directed multitarget drugs with antioxidant, cholinergic, neuroprotective and neurogenic properties, Eur. J. Med. Chem. 121 (2016) 376-386.

[38] M. Estrada Valencia, C. Herrera-Arozamena, L. de Andrés, C. Pérez, J.A. Morales-García, A. Pérez-Castillo, E. Ramos, A. Romero, D. Viña, M. Yáñez, E. Laurini, S. Pricl, M.I. Rodríguez-Franco, Neurogenic and neuroprotective donepezil-flavonoid hybrids with sigma-1 affinity and inhibition of key enzymes in Alzheimer's disease, Eur. J. Med. Chem. 156 (2018) 534-553.

[39] M. Estrada-Valencia, C. Herrera-Arozamena, C. Pérez, D. Viña, J.A. Morales-García, A. Pérez-Castillo, E. Ramos, A. Romero, E. Laurini, S. Pricl, M.I. Rodríguez-Franco, New

flavonoid – *N*,*N*-dibenzyl(*N*-methyl)amine hybrids: Multi-target-directed agents for Alzheimer´s disease endowed with neurogenic properties, J. Enzyme Inhib. Med. Chem. 34 (2019) 712-727.

[40] C. Herrera-Arozamena, M. Estrada-Valencia, C. Pérez, L. Lagartera, J.A. Morales-García, A. Pérez-Castillo, J.F. Franco-Gonzalez, P. Michalska, P. Duarte, R. León, M.G. López, A. Mills, F. Gago, Á.J. García-Yagüe, R. Fernández-Ginés, A. Cuadrado, M.I. Rodríguez-Franco, Tuning melatonin receptor subtype selectivity in oxadiazolone-based analogues: Discovery of QR2 ligands and NRF2 activators with neurogenic properties, Eur. J. Med. Chem. 190 (2020) 112090.

[41] F. Denizot, R. Lang, Rapid colorimetric assay for cell growth and survival: modifications to the tetrazolium dye procedure giving improved sensitivity and reliability, J. Immunol. Methods 89 (1986) 271-277.

[42] J. Jiaranaikulwanitch, P. Govitrapong, V.V. Fokin, O. Vajragupta, From BACE1 inhibitor to multifunctionality of tryptoline and tryptamine triazole derivatives for Alzheimer's disease, Molecules 17 (2012) 8312-8333.

[43] P. Purohit, I. Bruhova, S. Gupta, A. Auerbach, Catch-and-hold activation of muscle acetylcholine receptors having transmitter binding site mutations, Biophys. J. 107 (2014) 88-99.

[44] S.-J. Zuo, S. Zhang, S. Mao, X.-X. Xie, X. Xiao, M.-H. Xin, W. Xuan, Y.-Y. He, Y.-X. Cao, S.-Q. Zhang, Combination of 4-anilinoquinazoline, arylurea and tertiary amine moiety to discover novel anticancer agents, Bioorg. Med. Chem. 24 (2016) 179-190.

[45] G.A. Russell, K. Wang, Electron transfer processes. 53. Homolytic alkylation of enamines by electrophilic radicals, J. Org. Chem. 56 (1991) 3475-3479.

[46] K.D. Rice, N.K. Anand, A. Arcalas, C.M. Blazey, J. Bussenius, W.K.V. Chan, H. Du, S. Epshteyn, M.A. Ibrahim, P. Kearney, Pyrimidinones as casein kinase II (CK2) modulators, US Patent 20090215803A1 (Jan. 22, 2009).

[47] G.A. Molander, D.L. Sandrock, Aminomethylations via cross-coupling of potassium organotrifluoroborates with aryl bromides, Org. Lett. 9 (2007) 1597-1600.

[48] H.-R. Tsou, S. Ayral-Kaloustian, G.H. Birnberg, M.B. Floyd, J. Kaplan, K.M. Kutterer, X. Liu, R. Nilakantan, M.A. Otteng, Z. Tang, Substituted isoquinoline-1,3(2*H*,4*H*)-diones, 1-thioxo, 1,4-dihydro-2*H*-isoquinoline-3-ones and 1,4-dihyro-3(2*H*)-isoquinolones and methods of use thereof, US Patent 7,713,994 (May 11, 2010).

[49] R.J. Lukas, Characterization of curaremimetic neurotoxin binding sites on membrane fractions derived from the human medulloblastoma clonal line, TE671, J. Neurochem. 46 (1986) 1936-1941.

[50] C.G. Sharples, S. Kaiser, L. Soliakov, M.J. Marks, A.C. Collins, M. Washburn, E. Wright, J.A. Spencer, T. Gallagher, P. Whiteaker, UB-165: a novel nicotinic agonist with subtype selectivity implicates the α4β2* subtype in the modulation of dopamine release from rat striatal synaptosomes, J. Neurosci. 20 (2000) 2783-2791.

[51] M. Gopalakrishnan, L.M. Monteggia, D.J. Anderson, E.J. Molinari, M. Piattoni-Kaplan, D. Donnelly-Roberts, S.P. Arneric, J.P. Sullivan, Stable expression, pharmacologic properties and regulation of the human neuronal nicotinic acetylcholine alpha 4 beta 2 receptor, J. Pharmacol. Exp. Ther. 276 (1996) 289-297.

[52] L.M. Boland, M.M. Drzewiecki, G. Timoney, E. Casey, Inhibitory effects of polyunsaturated fatty acids on Kv4/KChIP potassium channels, Am. J. Physiol. Cell Physiol. 296 (2009) C1003-1014.

[53] A. Corbin-Leftwich, S.M. Mossadeq, J. Ha, I. Ruchala, A.H. Le, C.A. Villalba-Galea, Retigabine holds KV7 channels open and stabilizes the resting potential, J. Gen. Physiol. 147 (2016) 229-241.

Declaration of interests

☒ The authors declare that they have no known competing financial interests or personal relationships that could have appeared to influence the work reported in this paper.

☐The authors declare the following financial interests/personal relationships which may be considered as potential competing interests:

Optical control of muscular nicotinic channels with azocuroniums, photoswitchable azobenzenes bearing two *N*-methyl-*N*-carbocyclic quaternary ammonium groups

Clara Herrera-Arozamena[a], Martín Estrada-Valencia[a], Olaia Martí-Marí[a], Concepción Pérez[a], Mario de la Fuente Revenga[b], Carlos A. Villalba-Galea[c,*], and María Isabel Rodríguez-Franco[a,*]

[a]Instituto de Química Médica, Consejo Superior de Investigaciones Científicas (IQM-CSIC), c/ Juan de la Cierva 3, E-28006 Madrid, Spain.

[b]Department of Physiology and Biophysics, School of Medicine, Virginia Commonwealth University, Richmond, VA 23298, USA

[c]Physiology and Pharmacology Department, University of the Pacific, Stockton, CA, USA.